Available online at www.sciencedirect.com
SCIENCE DIRECT
Fluid Phase Equilibria 244 (2006) 193–211
FLUID PHASE EQUILIBRIA
www.elsevier.com/locate/fluid

Multiparameter equations of state for selected siloxanes☆

P. Colonna[a,*], N.R. Nannan[a], A. Guardone[b], E.W. Lemmon[c]

[a] *Process and Energy Department, Delft University of Technology, Leeghwaterstraat 44, 2628 CA Delft, The Netherlands*
[b] *Dipartimento di Ingegneria Aerospaziale, Politecnico di Milano, Via La Masa 34, 20154 Milano, Italy*
[c] *Physical and Chemical Properties Division, National Institute of Standards and Technology, 325 Broadway, Boulder, CO 80305, USA*

Received 9 January 2006; received in revised form 21 April 2006; accepted 25 April 2006

Abstract

This article presents the development of technical equations of state for four siloxanes using the 12-parameter Span–Wagner functional form. Siloxanes are used as heat transfer fluids and working media in energy conversion applications. The investigated fluids are two linear dimethylsiloxanes, namely MM (hexamethyldisiloxane, $C_6H_{18}OSi_2$) and MD_4M (tetradecamethylhexasiloxane, $C_{14}H_{42}O_5Si_6$), and two cyclic dimethylsiloxanes, namely D_4 (octamethylcyclotetrasiloxane, $C_8H_{24}O_4Si_4$) and D_5 (decamethylcyclopentasiloxane, $C_{10}H_{30}O_5Si_5$). Available measured properties are critically evaluated and selected for the optimization of the equation of state (EoS) parameters. Due to the insufficient number of experimental values, several other properties are estimated with the most accurate ad hoc methods. These estimates are included in the optimization of the equation of state parameters. Moreover, experimental saturated liquid density and vapor pressure data are correlated with the equations proposed by Daubert and Wagner–Ambrose, respectively, to provide short, simple, and accurate equations for the computation of these properties. The performance of the obtained equations of state is assessed by comparison with experimental data and also with estimates obtained with the Peng–Robinson cubic EoS with the modification proposed by Stryjek and Vera. This equation was adopted in previous technical studies. The improvements obtained with the newly developed EoS's are significant. Exemplary state diagrams are also reported as a demonstration of the consistency of the obtained thermodynamic models. Sound speed measurements in the vapor phase are planned for the near future and results will be incorporated in future improvements of the newly developed thermodynamic models.
© 2006 Elsevier B.V. All rights reserved.

PACS: 64.30.+t

Keywords: Caloric properties; Critical point; Density; Equation of state; Fundamental equation; Siloxane; Thermodynamic properties; Vapor pressure; D_4; D_5; MM; MD_4M

1. Introduction

Many energy conversion applications employ organic fluids as working media. Some of these organic fluids and their applications are listed in Table 1. Out of the class of organic fluids, siloxanes have some positive technological characteristics because of their low/non-toxicity, excellent thermal stability, limited flammability, and in the case of Organic Rankine Cycle (ORC) applications, good thermodynamic properties with respect to cycle design (see, e.g., Refs. [1–4]). Moreover, siloxanes are already bulk-produced, mainly for the cosmetics industry.

Another interesting aspect is that, due to their molecular complexity, siloxanes are candidate Bethe–Zel'dovich–Thompson (BZT) fluids and may thus exhibit non-classical gasdynamic behavior in the superheated region close to saturation at high reduced pressures and temperatures ($0.7 \leq P_r \leq 1$, $0.95 \leq T_r \leq 1.01$) [5,6]. Research is currently underway at the Energy Technology section, Delft University of Technology, regarding BZT behavior of fluids in the dense gas region and the use of these fluids in energy conversion applications: non-classical gasdynamic effects could be exploited for instance to improve the efficiency of ORC turbines [7]. The goal of the project is to provide experimental evidence of non-classical phenomena. For the design of the experimental setup and for the

☆ Contribution in part of the National Institute of Standards and Technology, not subject to copyright in the United States.

* Corresponding author. Tel.: +31 15 2782172; fax: +31 15 2782460.
E-mail address: p.colonna@tudelft.nl (P. Colonna).

0378-3812/$ – see front matter © 2006 Elsevier B.V. All rights reserved.
doi:10.1016/j.fluid.2006.04.015

Table 1
Energy conversion applications of organic fluids

Fluid class	Applications
Hydrocarbons	Expanders and compressors in (petro)chemical processes, geothermal Organic Rankine Cycles (ORC's)
Fluorocarbons	Refrigeration and air conditioning, geothermal ORC's, low-temperature heat recovery ORC's
Siloxanes	High-temperature ORC's, heat transfer fluids (possible future application: high-temperature heat pumps)

analysis of the results, an accurate and complete thermodynamic model for siloxanes is mandatory.

Accurate and consistent estimation of thermodynamic properties is of the outmost importance both in the design of advanced energy applications and in non-classical gasdynamic investigations. Equations of state are the choice for these applications at present: with modern equations of state, all thermodynamic properties of technical interest can be calculated with high accuracy and are thermodynamically consistent. The consistency of the thermodynamic model is a requirement for all complex numerical simulation codes. To the knowledge of the authors, a thermodynamic multiparameter model for siloxanes that is accurate over the entire thermodynamic range and for all thermodynamic properties is currently not available elsewhere and drove the present effort.

Siloxanes are a class of fluids composed of molecules containing alternate silicon and oxygen atoms in either a linear or cyclic arrangement usually with one or two organic groups attached to each silicon atom. For this work, cyclic molecules D_4 (octamethylcyclotetrasiloxane, $C_8H_{24}O_4Si_4$) and D_5 (decamethylcyclopentasiloxane, $C_{10}H_{30}O_5Si_5$) together with the linear molecule MD_4M (tetradecamethylhexasiloxane, $C_{14}H_{42}O_5Si_6$) were selected because of their possible application in non-classical gasdynamic studies [5]. In addition, the simplest linear siloxane MM (hexamethyldisiloxane, $C_6H_{18}OSi_2$) was selected because current Organic Rankine Cycle turbines employ the lighter compounds among the siloxane molecules. Nonetheless, in principle these siloxanes can all be used as working fluids in Organic Rankine Cycle turbines. The extension of this work to other light linear and cyclic siloxanes is planned for the near future.

Thermodynamic properties of siloxanes can be obtained with lower accuracy from equations of state using only critical point properties and the acentric factor as fluid parameters. Standard cubic equations of state (EoS) are examples. The use of the Peng–Robinson EoS modified by Stryjek and Vera (PRSV) to model siloxanes is documented in Ref. [2]. This EoS provides accurate estimates of the saturation pressures and can be used together with modern mixing rules to estimate the properties of mixtures (also in Ref. [2]), but suffers from the well known limitations of cubic equations of state, namely: (a) incorrect functional form at high subcritical reduced temperatures and pressures and in the superheated region close to the critical point, (b) low accuracy of saturated and subcooled liquid densities (especially for polar molecules). Moreover, given the very limited number of fluid parameters in the EoS, optimized cubic equations of state are inherently less accurate than optimized multiparameter equations of state for all of the thermodynamic properties, including vapor pressures.

The Span and Wagner multiparameter functional form [8,9] has been chosen to overcome these limitations in order to model pure siloxanes' properties over the whole thermodynamic range of interest for technical applications with the highest possible accuracy. An EoS based on the Span and Wagner functional form can generally represent thermodynamic data within the experimental uncertainty with which the considered properties are measured. Span and Wagner developed two fundamental equations with 12 terms: one is optimized for non-polar or slightly polar compounds and the other for polar fluids. The relatively small number of fluid parameters was carefully selected so that the thermodynamic constraints are more easily satisfied and the correct extrapolation behavior at high and low temperatures is also assured with proper fitting.

Another important advantage with respect to other highly accurate EoS's is that the limited number of parameters allows for faster computations. This is an important requirement if the software thermodynamic library in which the model is implemented is used to provide properties to computational fluid dynamics (CFD) programs [5,6] or dynamic systems simulations [10,11].

To successfully optimize the EoS parameters, a sufficient number of accurate experimental data must be available. The amount of such data for the siloxanes is quite limited and other experimental data that would be desirable include a greater number of saturated liquid and vapor density measurements. Moreover, in order to compute caloric properties, the knowledge of the isobaric ideal gas heat capacity is required. This constitutes one of the main sources of uncertainty for all the fluids except for MM. To overcome this problem, modern ad hoc estimation techniques were used to predict other necessary data to be included in the optimization of the EoS parameters. The uncertainty of such estimation methods is known; therefore, the assessment of the accuracy of the obtained EoS is also possible. Given the fitting ability of the Span and Wagner EoS, the values calculated with the EoS are at least as accurate as the values obtained with the ad hoc estimation techniques. Furthermore, superheated sound speed measurements for some of the selected siloxanes are planned for the near future.

The EoS's presented here constitute a fundamental starting point in the complex non-linear, constrained optimization problem, and improved accuracies can be obtained with a limited effort whenever additional experimental data become available. In any case, the EoS's described here can be used in technical applications, because the accuracy for all properties is well within common engineering requirements.

The available experimental properties for the considered siloxanes are assessed for consistency and are qualitatively evaluated in Section 2. Section 3 briefly describes the methods used to estimate saturated liquid and vapor densities and the isobaric ideal gas heat capacities. Results of the application of these methods are also presented. The Span–Wagner functional form is briefly reviewed in Section 4, which also contains a description of the parameter optimization method and the results of

the procedure, namely tables summarizing the EoS parameters for the considered siloxanes. The performance of the EoS's for MM, MD_4M, D_4, and D_5 is analyzed in Section 5. Since siloxanes were previously modeled to study thermodynamic cycles [2] using the Peng–Robinson cubic equation of state modified by Stryjek and Vera to obtain accurate saturation pressure estimates [12], the PRSV EoS is included in the performance evaluation of the newly obtain EoS's in the Span–Wagner functional form. Section 5.1 reports sample state diagrams obtained with the thermodynamic model implemented in a software program [13]. State diagrams show the consistency of the implemented model and the capacity of the program to calculate all the thermodynamic properties of technical interest over the entire range of validity of the model. State diagrams are a primary tool for the design of thermodynamic cycles. Section 5.2 reports the assessment of the performance of the new equations of state, i.e., calculated thermodynamic properties are compared with available experimental data. Relevant state points are computed with the FluidProp software package [13]. FluidProp allows for the computation of both volumetric and caloric properties, among which are the sound speed, derived properties used in computational fluid dynamics and dynamic simulations codes, and also the fundamental derivative of gas dynamics (see, e.g., Ref. [5]). Section 6 describes the sensitivity analysis performed to assess the influence of the uncertainty on the isobaric ideal gas heat capacity (C_P^{ig}) on the estimate of caloric properties. The uncertainty on the C_P^{ig} estimates for MD_4M, D_4, and D_5, which DIPPR [14] reports as 25%, is one of the main limitations of the developed models.

2. Available thermodynamic data

The available critical properties and the main thermodynamic parameters are reported in Tables 2 and 3 for the linear molecules and in Tables 4 and 5 for the cyclic molecules. The tables include experimental and estimated values and related uncertainties, if available. The tables show that the experimental values are somewhat scattered. An extensive assessment of siloxanes' critical properties is reported in Ref. [15]. The values used in this work are those selected by Flaningam and published in the DIPPR database [14]. Table 6 summarizes the selected critical values.

Other available experimental thermodynamic data for the selected fluids are summarized in Table 7. These data are qualitatively evaluated in the following section, i.e., they are checked for consistency by means of ad hoc estimation methods and by inspection of visual information provided by thermodynamic charts. A quantitative evaluation of the available experimental data is difficult because experimental data from different sources are not available.

2.1. Evaluation of experimental vapor pressure data and fluid parameters for the Wagner–Ambrose vapor pressure equation

Fig. 1 shows the available experimental vapor pressure data as a function of the measured temperature for all four fluids. The

Table 2
Thermodynamic properties and parameters (measured, estimated, or calculated) for fluid MM [16]

Property (unit)	Value	Source	Msd/Est/Calc
MW (kg/kmol)	162.37752	[14]	Calc
T_{TP} (K)	204.93	[18]	Msd
T_c (K)	518.75 ± 0.40	[15,14]	Msd
	518.70 ± 0.51	[19]	Msd
	516.6	[20]	Msd
	518.8	[21]	Msd
P_c (MPa)	1.939 ± 0.02	[14]	Est
	1.925 ± 0.01	[19]	Msd
	1.910	[20,21,22]	Msd
v_c (m^3/kmol)	0.629 ± 0.03	[23]	Msd
	0.5734	[20]	Msd
	0.601	[14]	Est
	0.573	[22]	Msd
	0.583	[21]	Msd
T_b (K)	373.67 ± 0.10	[14]	Msd
	373.65 ± 2	[19]	Msd
	373.70 ± 0.1	[24]	Msd
Δh_{vap} at T_b (kJ/kg)	192.5	[18]	Msd
ω	0.419	[14]	Calc
	0.413	[19]	Calc

Uncertainties are reported, if available [14,17].

Table 3
Thermodynamic properties and parameters (measured, estimated, or calculated) for fluid MD_4M [16]

Property (unit)	Value	Source	Msd/Est/Calc
MW (kg/kmol)	458.99328	[14]	Calc
T_{MP} (K)	214.15	[14]	Msd
T_c (K)	653.2 ± 1.2	[14,15,22]	Msd
P_c (MPa)	0.877 ± 0.02	[14]	Est
	0.804	[14,22]	Msd
v_c (m^3/kmol)	1.65	[14]	Est
	1.808	[14]	Msd
	1.723	[22]	Msd
T_b (K)	532.9 ± 0.20	[14]	Msd
Δh_{vap} at T_b (kJ/kg)	113	[25]	Msd
ω	0.785	[14]	Calc

Uncertainties are reported, if available [14,17].

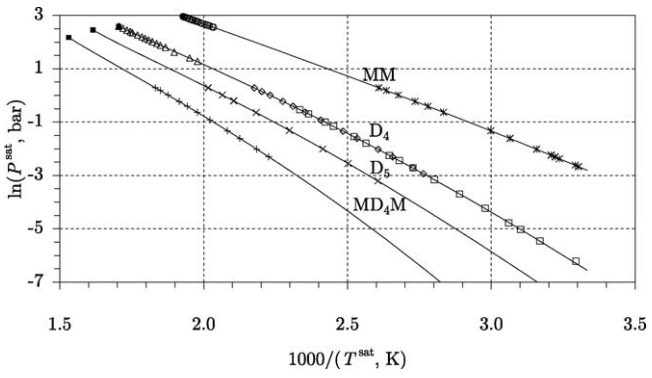

Fig. 1. Measured vapor pressure as a function of the saturation temperature. The data are correlated with the Wagner–Ambrose [37] vapor pressure equation.

Table 4
Thermodynamic properties and parameters (measured, estimated, or calculated) for fluid D_4 [16]

Property (unit)	Value	Source	Msd/Est/Calc
MW (kg/kmol)	296.61576	[14]	Calc
T_{TP} (K)	290.25 ± 0.02	[26]	Msd
T_c (K)	586.5	[14,15]	Msd
	585.7 ± 0.3	[23]	Msd
	586.5 ± 0.2	[20]	Msd
	587.15	[27,28]	Msd
P_c (MPa)	1.332	[14]	Est
	1.32 ± 0.02	[23]	Msd
	1.33959 ± 0.00686	[20]	Msd
	1.324	[29]	Msd
	1.420	[27]	Msd
v_c (m^3/kmol)	0.970	[14]	Est
	0.984	[20]	Msd
	0.910	[29]	Msd
ρ_c (kmol/m^3)	0.995 ± 0.00991	[23]	Msd
T_b (K)	448.15	[14]	Msd
	446.2 ± 0.6	[30]	Msd
Δh_{vap} at T_b (kJ/kg)	126.8	[27]	Msd
ω	0.5890	[14]	Calc

Uncertainties are reported, if available [14,17].

uncertainties of the experimental values are indicated in Table 8. Fig. 1 also shows the regression of the available experimental data with the Wagner–Ambrose vapor pressure equation [37,38] given by:

$$\ln P_r^{sat} = \frac{\omega_1 \tau_* + \omega_2 \tau_*^{1.5} + \omega_3 \tau_*^{2.5} + \omega_4 \tau_*^5}{T_r^{sat}}, \quad (1)$$

where $\tau_* = 1 - T_r^{sat}$. In the expression above, $T_r^{sat} = T^{sat}/T_c$, where T^{sat} and T_c are the saturation and critical temperature, respectively, and $P_r^{sat} = P^{sat}/P_c$, where P^{sat} and P_c are the saturation and critical pressure, respectively. The constants a, b, c, and d are substance-dependent parameters that are obtained by fitting Eq. (1) to the available experimental data. Table 9 reports parameters a–d for MM, MD_4M, D_4, and D_5. These parameters

Table 5
Thermodynamic properties and parameters (measured, estimated, or calculated) for fluid D_5 [16]

Property (unit)	Value	Source	Msd/Est/Calc
MW (kg/kmol)	370.7697	[14]	Calc
T_{TP} (K)	226 ± 1.0	[31]	Msd
T_c (K)	619.15	[14,15]	Est
	617.4 ± 0.3	[23]	Msd
P_c (MPa)	1.160	[14,15]	Est
	1.035 ± 0.02	[23]	Msd
v_c (m^3/kmol)	1.216	[14]	Est
ρ_c (kmol/m^3)	0.777 ± 0.00774	[23]	Msd
T_b (K)	484.1	[14,15]	Msd
Δh_{vap} at T_b (kJ/kg)	121.3	[25]	Msd
ω	0.6658	[14]	Calc

Uncertainties are reported, if available [14,17].

Table 6
Critical properties used in the EoS's [14,17]

Fluid	Property (unit)	Value	Estimated uncertainty (%) [14]
MM	Critical temperature (K)	518.75	<3
	Critical pressure (MPa)	1.939	<5
	Critical specific volume (m^3/kmol)	0.629	<25
MD_4M	Critical temperature (K)	653.2	<3
	Critical pressure (MPa)	0.877	<10
	Critical specific volume (m^3/kmol)	1.65	<10
D_4	Critical temperature (K)	586.5	<1
	Critical pressure (MPa)	1.332	<3
	Critical specific volume (m^3/kmol)	0.970	<5
D_5	Critical temperature (K)	619.15	<5
	Critical pressure (MPa)	1.160	<10
	Critical specific volume (m^3/kmol)	1.216	<10

Table 7
Summary of experimental data for the selected siloxanes [16]

Fluid	Data type[a]	P range (bar)	T range (K)	No. of points	Source
MM	P^{sat}	–	302–519	26	[15,18,19]
	C_P^L	–	208–371	20	[18]
	P–ρ–T	0.6–3	448–573	43	[24]
		1.01325	278–358	13	[32]
MD_4M	P^{sat}	–	449–546	11	[15]
	P–ρ–T	1.01325	298–412	19	[32]
D_4	P^{sat}	–	303–586	45	[15,20,27]
	ρ^L	–	292–576	21	[20,33]
	ρ^V	–	505–580	10	[20]
	c^L	–	303–440	18	[34]
	c	1×10^{-3} to 600	300–450	135	[34]
	P–ρ–T	1–1800	308–427	42	[35,36]
D_5	P^{sat}	–	383–496	8	[15]
	ρ^L	–	302–451	21	[33]

[a] Superscripts 'L' and 'V' indicate saturated liquid and vapor, respectively, superscript 'sat' stands for saturated, and c is the speed of sound.

are calculated by considering all available experimental data and using the critical temperatures and pressures reported in Table 6.

Poling et al. [38] compared many different vapor pressure correlations, e.g., the Antoine equation, Riedel's corresponding-states method, etc., for acetone, 1-octanol, and *n*-tetradecane.

Table 8
Experimental uncertainty for the published vapor pressure measurements

Fluid name	Source	$\varepsilon(T^{sat})$ (K)	$\varepsilon(P^{sat})$
MM	[15]	0.01	0.07%
	[18]	Uncertainty could not be established	
	[19]	0.05	0.01 MPa
MD_4M	[15]	0.01	0.07%
D_4	[15]	0.01	0.07%
	[27]	Uncertainty could not be established	
	[20]	0.2	0.07 bar
D_5	[15]	0.01	0.07%

Table 9
Parameters $\omega_1 - \omega_4$ for the Wagner–Ambrose vapor pressure equation [Eq. (1)]

Fluid name	ω_1	ω_2	ω_3	ω_4
MM	−7.3380	−0.30930	0.20125	−13.455
MD_4M	−10.2921	3.3035	−8.0592	−2.4366
D_4	−8.8952	2.5694	−6.3275	−3.5483
D_5	−9.4473	3.0697	−6.9411	−2.1692

Critical properties are taken from Ref. [14] (see Table 6).

Their results show that, since the Wagner–Ambrose equation has the largest number of correlated parameters, it is the most accurate for temperatures from the triple point up to the critical temperature and has the best extrapolation behavior. The Wagner–Ambrose vapor pressure equation is therefore preferable with respect to the corresponding-states method of Riedel [38] (AIChE DIPPR equation) selected by Flaningam [15].

Fig. 1 shows that the data points can be smoothly interpolated with Eq. (1). A closer inspection of the absolute deviations between the values calculated using Eq. (1) and the experimental data indicates however, that for some of the values deviations are greater than 3%. These fluctuations in the deviations might be an indication that these particular experimental values are affected by some error, and therefore they were discarded in the optimization of the EoS parameters. On average, all experimental vapor pressures are predicted by Eq. (1) within 1%.

2.2. Evaluation of saturated liquid specific volume data

Experimental saturated liquid specific volume data are available only for D_4 [20,33] and D_5 [33]. The average uncertainty in the experimental specific volume data and their related saturation temperatures, as reported by Young [20], are approximately 0.3% and 0.2 K, respectively. For the data reported in Ref. [33], the average uncertainties are less than 0.2% in density.

The modified Rackett equation [38] was chosen to evaluate the saturated liquid specific volume data for D_4 reported in the literature. The modified Rackett equation provides a generalized correlation for computing saturated liquid specific volumes and is given by:

$$v^{\mathrm{L}} = v_{\mathrm{c}} Z_{\mathrm{c}}^{(1-(T/T_{\mathrm{c}}))^{2/7}}, \tag{2}$$

where Z is the compressibility factor. The subscript 'c' stands for properties evaluated at the critical point and the superscript 'L' indicates the saturated liquid phase.

According to Smith et al. [39], values calculated with Eq. (2) are usually accurate to within 1–2%, but deviations with respect to experimental data can be as high as 5%, depending on the accuracy of the critical properties. The experimental data deviate from the densities computed with the Rackett equation and the chosen critical point (Table 6) by less than 5% and with an average absolute deviation (AAD) of 3.7%. The experimental data appear to be qualitatively consistent because all deviations are of the same order of magnitude and do not fluctuate significantly. The larger deviation with respect to the values suggested by Smith et al. can possibly be attributed to the low accuracy of the critical point data. All of the saturated liquid specific volume data for D_4 were used in the optimization of the Span–Wagner EoS parameters.

If the Rackett equation is used to correlate the experimental data reported in Ref. [33] for D_5, the observed deviations are significantly larger (about 6.5%). In this case the critical properties used in Eq. (2) might be considerably less accurate than for D_4. This deduction is confirmed by observing that the available critical point data for D_5 are comparatively more scattered (see Table 5) and particularly the reported critical pressures deviate by approximately 12% and the critical specific volumes by about 6%.

The equation proposed by Daubert et al. (Ref. [38]) is used to further investigate the reported data. The Daubert equation can be written as:

$$v^{\mathrm{L}} = \frac{B^{1+(1-T^{\mathrm{sat}}/C)^D}}{A}, \tag{3}$$

where A, B, C, and D are adjustable parameters, and can be determined by fitting the functional form to the available experimental data. This avoids using the critical point data, which can cause higher deviations. The following values are usually taken as initial guesses for the fitting procedure: C is set equal to the critical temperature, and A, B, and D are set to $P_{\mathrm{c}}/RT_{\mathrm{c}}$, Z_{c}, and 2/7, respectively. If the critical property data provided in Ref. [14] are used as the initial guess, the resulting coefficients are $A = 83.770\,\mathrm{kg/m^3}$, $B = 0.26293$, $C = 619.09\,\mathrm{K}$, and $D = 0.3041$. With these values, the AAD between experimental and calculated saturated liquid specific volumes is 0.07%. The saturated liquid specific volumes reported in Ref. [33] thus appear to be consistent and all data were used in the Span–Wagner EoS parameters' optimization. The application of the Daubert equation does not help in discriminating between the best measurements for the critical point of D_5.

2.3. Evaluation of saturated vapor density data

Saturated vapor density data are available only for D_4 [20]. The reported measurements are taken at high values of reduced temperature ($0.86 \leq T_{\mathrm{r}} \leq 0.99$), and the author indicates an uncertainty of 0.5%.

The principle of corresponding-states is employed to evaluate these experimental data. Dodecane ($C_{12}H_{26}$) is chosen as the reference fluid for the application of the corresponding-states principle to D_4, because its properties are well known [40] and because it has similar values for the critical compressibility and for the acentric factor (the critical compressibility factor is 0.27[1] and 0.25 for D_4 and dodecane, respectively, and the acentric factor is 0.589 for D_4 and 0.575 for dodecane). The application of the principle of corresponding-states indicates that the saturated vapor densities reported in Ref. [20] contain a systematic error, as can be seen in Fig. 2.

To confirm this finding, saturated vapor densities are also computed by making use of the Peng–Robinson EoS with the

[1] Estimated from critical point data in Ref. [14].

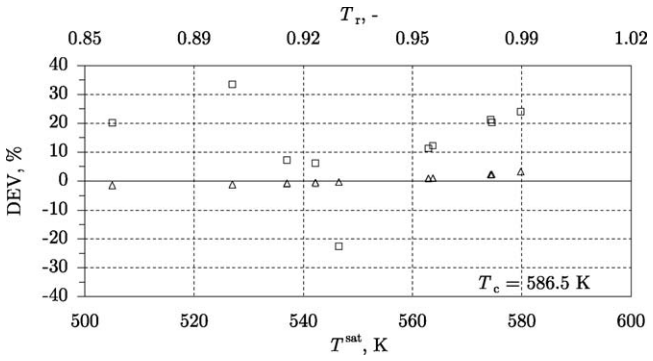

Fig. 2. Deviations between saturated vapor densities for D_4. Base values are calculated with the corresponding-states principle (reference fluid: dodecane). (△) Deviations with values computed using the PRSV EoS, i.e., $100((\rho^V_{PRSV} - \rho^V_{CS})/(\rho^V_{CS}))$ and (□) deviations with data published in Ref. [20], i.e., $100((\rho^V_{exp} - \rho^V_{CS})/(\rho^V_{CS}))$.

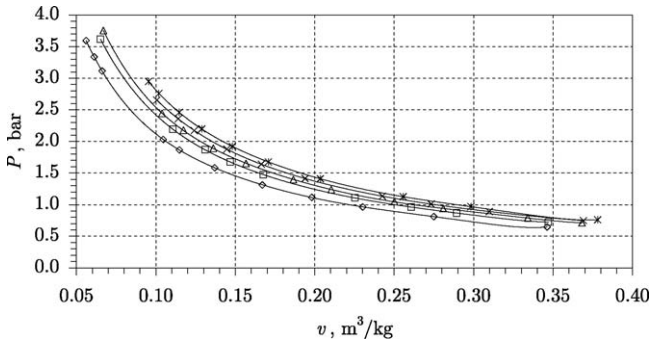

Fig. 3. Superheated vapor isotherms in the P–v plane for MM using experimental data reported in Ref. [24]. (⋆) T = 573.04 K; (×) T = 548.04 K; (△) T = 523.15 K; (□) T = 498.28 K; (◇) T = 448.26 K.

Stryjek–Vera modification (see Refs. [2,12]). The PRSV EoS is optimized to obtain accurate estimations of vapor pressures. Peng–Robinson type equations of state in general predict saturated vapor densities within a few percent of the experimental value up to $P_r = 0.9$ (see, e.g., Refs. [41,42]). As depicted in Fig. 2, the values calculated with the PRSV EoS agree within 3.5% with the values obtained by application of the corresponding-states principle, while the data reported in Ref. [20] deviate by as much as 32%; therefore, the latter were not used in the procedure to optimize the Span–Wagner EoS parameters.

2.4. Evaluation of vapor and liquid P–v–T data

Vapor phase P–v–T measurements are available only for MM [24]. The uncertainty indicated by the authors is 0.33 kPa for pressures and 0.1 K for temperatures. The uncertainty in the density could not be established. Atmospheric subcooled liquid specific volumes for MM and MD_4M are reported in Ref. [32]. These authors indicate that the uncertainty in the specific volume data is 0.00005 cm^3/g and show that the data are consistent. Isothermal subcooled liquid densities are reported only for D_4: in Ref. [35] the authors state that their measurements are accurate to within 0.4%. Atmospheric subcooled liquid densities for D_4 are documented in Ref. [36], but no uncertainty is reported.

Fig. 3 illustrates measured superheated isotherms in the P–v plane for MM. The experimental points are also interpolated by means of polynomial curves. All data points reported by Marcos et al. [24] appear to be consistent and were therefore used in the procedure for optimizing the Span–Wagner EoS parameters.

Fig. 4 shows a qualitative evaluation of the liquid P–v–T data by Wappmann et al. for D_4 [35]: for a given isotherm, the molar density is plotted as a function of the pressure. All of the data points can be smoothly interpolated with a polynomial curve. Thus from a qualitative point of view, all of the measured data points of Wappmann et al. are consistent. Additional P–v–T data for D_4 are provided by Benson and Winnick [36]: at a pressure of 1 atm, the specific volume is measured at different temperatures. The PRSV EoS has been chosen to verify the reported experimental values because cubic equations of state are known to predict low pressure subcooled liquid densities for non-polar or slightly polar substances with reasonable accuracy [41]. For the given pressure and temperature, the specific volume is computed and compared with the experimental value. The maximum deviation between the experimental and computed values is less than 1%. All of the reported subcooled liquid densities for D_4 were therefore employed in the procedure to optimize the Span–Wagner EoS parameters.

2.5. Evaluation of heat capacity data

Experimental values for the isobaric heat capacity in the saturated liquid (C^L_P) and the ideal gas (C^{ig}_P) states are available only for MM [18]. These values were obtained from 363 to 500 K. Spectroscopic and molecular structure information were used to calculate C^{ig}_P from 273.15 to 1500 K by means of statistical mechanics. The calculated and experimental values are in good agreement, and the uncertainty of the obtained C^{ig}_P values is estimated to be <1% [14]. C^L_P values were measured from 209 to 371 K with an estimated accuracy of <3% and were fitted by the authors with a polynomial function. All of the available heat capacity data were therefore used to fit the parameters of the equation of state for MM.

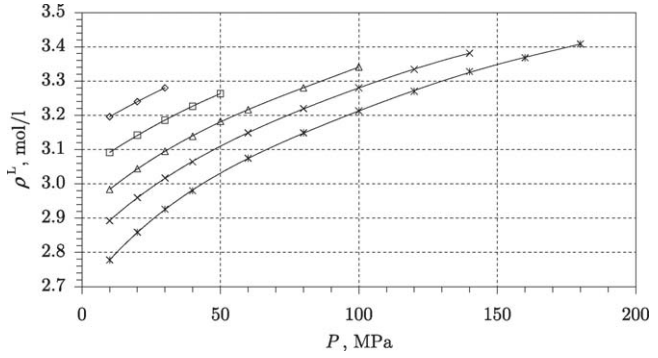

Fig. 4. Experimental molar densities as a function of pressure along isotherms in the subcooled liquid phase for D_4 [35]. (◇) T = 308.2 K; (□) T = 337.7 K; (△) T = 367.9 K; (×) T = 394.9 K; (⋆) T = 426.6 K.

2.6. Evaluation of liquid sound speed data

Data for the speed of sound in the saturated and subcooled liquid phase are available only for D_4 and were reported by Niepmann and Schmidt [34] (the uncertainty according to the authors is ±0.8 m/s). These data were not included in the parameters' optimization procedure so that the speed of sound estimates obtained with the equation of state could be used to qualitatively evaluate their consistency a posteriori as a further test of the extrapolation capability of the Span–Wagner functional form. The comparison between the experimental sound speed data in the liquid state and the values calculated with the obtained equation of state are reported in Section 5.2.3.

3. Estimation of other thermodynamic properties for use in the optimization of the EoS parameters

As stated in Section 1, the amount of published experimental data is not sufficient to fit the parameters of the equations of state in the Span–Wagner functional form. To fill this gap, several ad hoc methods were used to increase the number of thermodynamic properties that are used in the optimization. As detailed below, estimated data are obtained for: (1) saturated vapor densities, (2) saturated liquid densities, and (3) isobaric ideal gas heat capacities.

3.1. Estimated saturated vapor densities

As detailed in Section 2.3, the only available experimental saturated vapor densities were discarded, therefore the PRSV EoS (see Ref. [2]) was employed to estimate saturated vapor densities for all fluids up to $P_r = 0.9$. Cubic equations of state yield saturated vapor densities that are accurate to within a few percent for non-polar or slightly polar molecules [41,42]. This finding is confirmed by numerous calculations done for hydrocarbons with a molecular structure similar to the considered siloxanes. Parameters for the PRSV EoS were obtained from the same critical data adopted in this work (see Table 6), with acentric factors published in the DIPPR database [14] and with the additional adjustable parameter k_1 optimized by use of the Wagner–Ambrose vapor pressure equation (parameters are given in Table 9). Saturated vapor densities were estimated for temperature increments of 10 K up to a temperature corresponding to a reduced pressure of 0.9.

3.2. Estimated saturated liquid densities

Although the number of experimental saturated liquid densities for D_4 is not very large, additional densities were not estimated because data were measured over a broad range of temperatures, namely $0.49 < T_r < 0.98$.

In the case of D_5, experimental saturated liquid density data are available over a much smaller temperature range ($0.49 < T_r < 0.73$); therefore, additional data were estimated with Eq. (3) and they are expected to be accurate to within 2% for $T_r < 0.97$.

Saturated liquid density measurements are not found in the literature for MM and MD_4M, therefore the Rackett equation was used to estimate values up to a reduced pressure of 0.9. As mentioned in Section 2.2, the accuracy of these estimates depends on the accuracy of the adopted critical values: the accuracy can be as good as 1–2% if the critical values are accurately known.

3.3. Isobaric ideal gas heat capacities

Experimental data are available only for MM, therefore the Harrison–Seaton zeroth order group contribution method [43] was used to estimate values for MD_4M, D_4, and D_5 in the range $300 \le T \le 673$ K. The lower temperature limit is 300 K, because Harrison and Seaton list only values for different groups between 300 and 1500 K. The upper temperature limit is based on the thermal stability value estimated from tests in stainless steel as the containing material [44], i.e., approximately 673 K (400 °C). Other advanced and more accurate estimation methods for C_P^{ig}, e.g., the Benson group contribution method [38] or the Constantinou and Gani method [38], cannot be used because the Si–C bond is not tabulated. In fact, according to Poling et al. [38], the Harrison–Seaton group contribution method is the only available technique to estimate isobaric ideal gas heat capacities for siloxanes. The uncertainty in the Harrison–Seaton group contribution method, when applied to siloxanes, is estimated at 25% [14].

All data were fitted with the polynomial expression given by:

$$C_P^{ig} = \eta_1 + \eta_2 T + \eta_3 T^2 + \eta_4 T^3. \quad (4)$$

Table 10 gives the values for the coefficients α–η for the selected siloxanes. In Eq. (4), T is in K and C_P^{ig} is in kJ/(kmol K).

The Aly–Lee equation [45] could also have been adopted instead of Eq. (4) [14]. The Aly–Lee equation is a self-consistent equation derived from the theory of statistical thermodynamics,

Table 10
Parameters $\eta_1 - \eta_4$ in Eq. (4) for the selected siloxanes

Fluid	η_1	η_2	η_3	η_4
MM[a]	51.894	741.34×10^{-3}	-416×10^{-6}	70.00×10^{-9}
MD_4M	−20.071	2228.5×10^{-3}	-1311.4×10^{-6}	286.2×10^{-9}
D_4	−18.256	1427.2×10^{-3}	-990.20×10^{-6}	300.0×10^{-9}
D_5	−34.898	1861.5×10^{-3}	-1403.4×10^{-6}	500.0×10^{-9}

$C_P^{ig} > 0$ for $300 \le T \le 673$ K.
[a] The range of validity is for $273 \le T \le 673$ K.

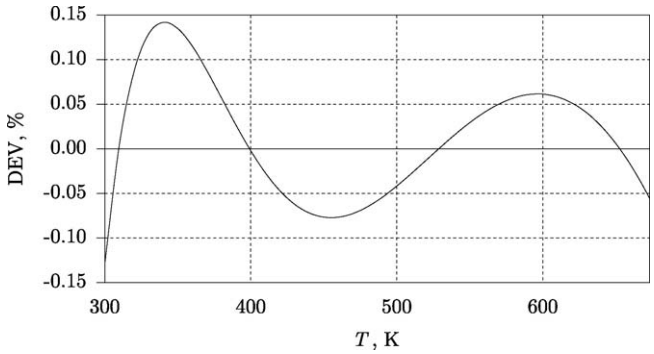

Fig. 5. Percentage deviations between C_P^{ig} values calculated with the Aly–Lee equation [45] and with Eq. (4) for MM in the validity range for the EoS ($300 < T < 673$ K). The Aly–Lee equation is taken as the base line.

and would have been preferable because Eq. (4) is empirical. Fig. 5 compares values obtained with the Aly–Lee equation and Eq. (4) for MM. The results indicate that the deviation between these two correlations is well within 0.15% for temperatures between 300 K and the upper temperature limit for the thermodynamic models. The polynomial equation is therefore chosen for simplicity.

4. Functional form of the equations of state and procedure for the optimization of the parameters

4.1. The Span–Wagner functional form for non-polar and weakly polar fluids

The new class of 12-parameter equations of state developed by Span and Wagner [8,46,47] is expressed in terms of the Helmholtz energy in the reduced form, i.e., $\Psi(T, \rho)/RT$, where Ψ is the specific Helmholtz energy and R is the universal gas constant, $R = 8.314472$ J/(mol K). To account for real gas effects, the reduced Helmholtz energy is split into a part that describes the ideal gas behavior and another part that takes into account the influence of intermolecular forces:

$$\frac{\Psi(T,\rho)}{RT} = \frac{\Psi^{ig}(T,\rho) + \Psi^{r}(T,\rho)}{RT} = \psi^{ig}(\tau,\delta) + \psi^{r}(\tau,\delta), \qquad (5)$$

where superscripts 'ig' and 'r' are abbreviations for ideal gas and residual, respectively, and δ and τ represent the dimensionless density $\delta = \rho/\rho_{ref}$ and the inverse dimensionless temperature $\tau = T_{ref}/T$. Usually the reference variables ρ_{ref} and T_{ref} are the critical values of the density and the temperature. The ideal gas Helmholtz energy is obtained from the isobaric ideal gas heat capacity correlation by considering that

$$\Psi^{ig} = \Psi_0 + \int_{T_0}^{T} (C_P^{ig} - R)\,dT - T\int_{T_0}^{T} \frac{C_P^{ig} - R}{T}\,dT + RT\,\ln\left(\frac{\rho}{\rho_0}\right). \qquad (6)$$

Subscript 0 refers to an arbitrarily chosen reference state. For the residual Helmholtz energy, Span and Wagner give the following functional form valid for non-polar and weakly polar fluids:

$$\begin{aligned}\psi^{r}(\tau,\delta) = {} & n_1\delta\tau^{0.250} + n_2\delta\tau^{1.125} + n_3\delta\tau^{1.500} + n_4\delta^2\tau^{1.375} \\ & + n_5\delta^3\tau^{0.250} + n_6\delta^7\tau^{0.875} + n_7\delta^2\tau^{0.625}\,e^{-\delta} \\ & + n_8\delta^5\tau^{1.750}\,e^{-\delta} + n_9\delta\tau^{3.625}\,e^{-\delta^2} \\ & + n_{10}\delta^4\tau^{3.625}\,e^{-\delta^2} + n_{11}\delta^3\tau^{14.5}\,e^{-\delta^3} \\ & + n_{12}\delta^4\tau^{12.0}\,e^{-\delta^3}, \end{aligned} \qquad (7)$$

where $n_1, \ldots, n_{12}$ are substance-specific parameters. The functional form given by Eq. (7) was devised by use of a sophisticated optimization algorithm that considered simultaneously sets of data for different fluids belonging to a certain group. The result of this procedure, namely the functional form, constitutes the basis for the development of numerically stable and accurate equations of state, valid for a certain group of fluids. Another positive characteristic is that the correct thermodynamic behavior is generally assured and the extrapolation behavior is very good. Equations of state derived from the Span–Wagner functional form are usually able to predict thermodynamic properties within the experimental uncertainty of the considered properties and can be used as reference EoS's.

4.2. Method to compute the parameters in the residual Helmholtz function

From a mathematical point of view, the calculation of the parameters in Eq. (7) for a certain fluid is a non-linear constrained minimization problem. The objective function is the weighted sum of the square of the deviations between experimental (or estimated) thermodynamic properties and values calculated with the equation of state. The overall accuracy of the obtained EoS depends on the accuracy of the experimental data that are used for its development, therefore weighting experimental data is necessary, since accurate data should contribute more to the final solution than less accurate data. Furthermore, experimental data with uncertainties larger than required should be discarded, or, when no or insufficient data are available for a certain region, the data should be weighted with their experimental or estimated uncertainties. For substances for which reliable data are not available in the critical region, Span and Wagner [8] propose including in the optimization process two estimated experimental saturated points with low weights. Taking as a reference the critical temperature, which is usually the most reliable critical property, the two points are

$$\rho^{V} = 0.9\rho_c, \qquad T = 0.9998T_c,$$
$$\rho^{L} = 1.1\rho_c, \qquad T = 0.9998T_c.$$

With these estimates and the experimental values for all three critical properties, the optimization procedure can be started.

The computational procedure is not deterministic and requires a certain amount of judgement and trials. A well-established program developed at NIST [9,40] was used for the optimization of the parameters for the selected siloxanes.

Table 11
Parameters $n_1, \ldots, n_{12}$ in Eq. (7) for MM

i	n_i	i	n_i
1	1.01686012	7	0.62845950
2	−2.19713029	8	$0.30903042 \times 10^{-1}$
3	0.75443188	9	−0.83948727
4	−0.68003426	10	−0.20262381
5	0.19082162	11	$-0.35131597 \times 10^{-1}$
6	$0.10530133 \times 10^{-2}$	12	$0.25902341 \times 10^{-1}$

Table 12
Parameters $n_1, \ldots, n_{12}$ in Eq. (7) for MD_4M

i	n_i	i	n_i
1	1.18492421	7	1.23544082
2	−1.87465636	8	$0.49462708 \times 10^{-1}$
3	$-0.65713510 \times 10^{-1}$	9	−0.73685283
4	−0.61812689	10	−0.19991438
5	0.19535804	11	$-0.55118673 \times 10^{-1}$
6	$0.50678740 \times 10^{-3}$	12	$0.28325885 \times 10^{-1}$

Table 13
Parameters $n_1, \ldots, n_{12}$ in Eq. (7) for D_4

i	n_i	i	n_i
1	1.05392408	7	0.70301835
2	−2.22981918	8	$0.47851888 \times 10^{-1}$
3	0.77573923	9	−0.80253480
4	−0.69374050	10	−0.18968872
5	0.18721557	11	$-0.22211781 \times 10^{-1}$
6	$0.42193330 \times 10^{-3}$	12	$0.60103354 \times 10^{-2}$

4.3. Results of the optimization procedure

The multiparameter constrained optimization, using the selected experimental and estimated data, provides the parameters $n_1, \ldots, n_{12}$ of the residual part of the Helmholtz energy equation of state [Eq. (7)]. The coefficients are listed in Tables 11–14. The reference values that were used to reduce the temperature and density in Eq. (7) are listed in Table 15. The reference state where the enthalpy and entropy are equal to zero is the saturated liquid phase at the normal boiling point temperature. The normal boiling point temperatures are also listed in Table 15.

The EoS's for MM, MD_4M, D_4, and D_5 are intended for technical use, therefore the range of validity is set for temperatures from 300 K up to the estimated thermal stability limit associated with stainless steel [44], i.e., 673 K. For MM the lower temperature limit is 273 K. The minimum temperature limit is based on the range of validity of the isobaric ideal gas heat capacity correlation, i.e., C_P^{ig}, that is required for computing caloric properties. The maximum pressure is arbitrarily set to 300 bar; the boundary is based on the limited technical interest of pressures greater than 300 bar for these fluids at present.

Table 14
Parameters $n_1, \ldots, n_{12}$ in Eq. (7) for D_5

i	n_i	i	n_i
1	1.40844725	7	0.82412481
2	−2.29248044	8	0.15214274
3	0.42851607	9	−0.68495890
4	−0.73506382	10	$-0.55703624 \times 10^{-1}$
5	0.16103808	11	$0.13055391 \times 10^{-1}$
6	$0.29643278 \times 10^{-3}$	12	$-0.31853761 \times 10^{-1}$

Table 15
Reducing variables for the equations of state and normal boiling point temperatures, and the critical pressures determined from the EoS in the Span–Wagner functional form for the selected siloxanes

Fluid	T_c (K)	P_c (bar)	ρ_c (mol/l)	T_b (K)
MM	518.69997204	19.3939	1.87467076	373.401
MD_4M	653.20000000	8.7747	0.62235694	532.723
D_4	586.49127187	13.3200	1.03512231	448.504
D_5	619.23462341	11.6146	0.78909027	484.050

Using the parameters $n_1, \ldots, n_{12}$ and α–η (see Table 10), all thermodynamic properties can be obtained through combinations of the Helmholtz energy function and its derivatives with respect to density and/or temperature. The performance of the obtained thermodynamic models is assessed in the following section.

5. Results

5.1. State diagrams

Figs. 6 and 7 show the P–v and T–s diagrams for D_4 as examples that demonstrate the consistency and capability of the thermodynamic model to calculate thermodynamic properties of technical interest over the range of validity of the thermody-

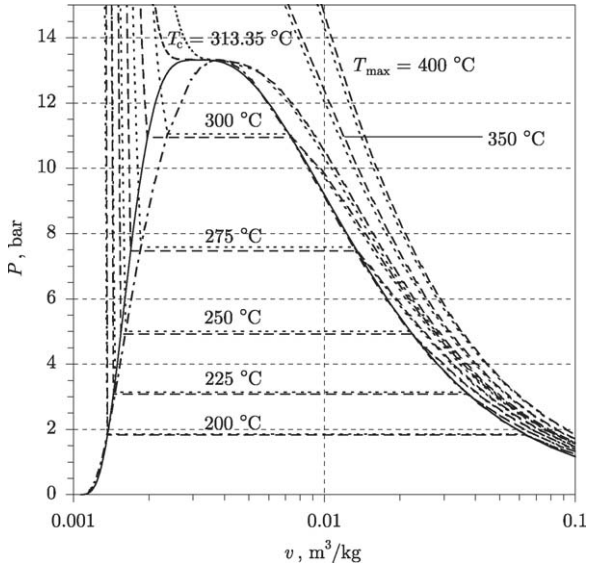

Fig. 6. P–v diagram for D_4 showing the saturation lines and several isotherms: comparison between properties calculated with the PRSV EoS [12] (with ··· and - · - denoting isotherms and the saturation curve, respectively) and the newly developed Span–Wagner functional form (- - - and —).

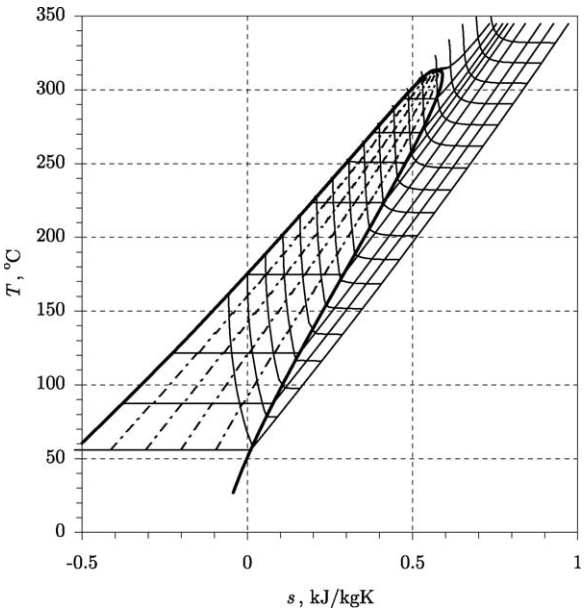

Fig. 7. T–s diagram for D_4 computed using the new Span–Wagner EoS showing several isobars (P = 0.01, 0.05, 0.2, 1, 3, 5, 7, 10, P_c [bar]), iso-quality lines (x = 0.2, 0.4, 0.6, and 0.8), and enthalpies (h = −25, 0, . . ., 375, 400 [kJ/kg]).

namic model. The state diagrams for MM, MD_4M, and D_5 are similar to the ones presented for D_4.

Fig. 6 also shows a graphical comparison with the PRSV EoS and shows the well known limitation of cubic equations of state to model the flat curvature of the saturation line close to the critical point. Furthermore, the PRSV EoS significantly over-predicts the saturated liquid specific volume data as the temperature increases up to its critical point value. However, because of the unavailability of experimental saturated vapor specific volume data (v^V) for all four siloxanes, the parameters $n_1, \ldots, n_{12}$ in the Span–Wagner functional form were optimized by including several values of v^V obtained with the PRSV EoS up to a reduced pressure of 0.9. This implies that on the vapor side the Span–Wagner EoS's have the same order of uncertainty as the PRSV cubic EoS.

In Fig. 7, it is worthwhile to note that, due to their large heat capacity (a consequence of the molecular complexity), siloxanes exhibit the so-called retrograde behavior in the vapor phase: the fluid remains dry upon expansion from saturated vapor conditions, except for a small thermodynamic region close to the critical point.

5.2. Performance evaluation

For a quantitative evaluation of the performance, the values of volumetric and caloric properties obtained using the newly developed EoS's in the Span–Wagner functional form (SW EoS) are compared with available experimental data and with values obtained with the PRSV cubic EoS. The evaluated thermodynamic properties include (if available): (a) the critical point, (b) vapor pressures, (c) saturated vapor and liquid densities, (d) gas and liquid phase P–v–T data, (e) gas and liquid phase sound speed data, and (f) gas and liquid phase heat capacity data.

5.2.1. Hexamethyldisiloxane, MM ($C_6H_{18}OSi_2$)

Available experimental data for MM include critical point data, vapor pressures, saturated liquid and low pressure subcooled isobaric heat capacities, and low pressure gas and liquid phase P–v–T data.

- *Critical point*. For the computation of the EoS parameters n_1, . . ., n_{12} in Eq. (7) for the selected siloxanes, the critical pressure and temperature are constrained to available experimental or estimated values by using appropriate weights while the critical specific volume is allowed to float, i.e., v_c is computed from the equation of state once the parameters are optimized. The experimental value for v_c is used as an initial estimate for the constrained optimization. Note that, for the selected siloxanes, the critical temperature datum is more reliable and accurate if compared to the value for P_c.

  Table 16 lists the deviation between the obtained value for v_c from the EoS and the values listed in the DIPPR database [14]. The uncertainty in the value for the critical specific volume is also indicated. Because of the comparatively large uncertainty in the literature value for v_c, the critical specific volume as computed from the Span–Wagner EoS for MM is reasonable, since the computed critical specific volume is within the estimated uncertainty of the experimental value.
- *Vapor pressure*. Deviations between experimental values and values calculated with the SW EoS for MM are reported in Fig. 8. Deviations with values calculated with the PRSV cubic EoS are also reported for comparison. The average absolute deviation between experimental and calculated data is approximately 0.53% for the SW EoS and 0.72% for the PRSV EoS. The improvement with respect to the PRSV EoS is not dramatic since the PRSV EoS is especially optimized to obtain accurate saturation pressure estimates.
- *Liquid phase isobaric heat capacity*. Fig. 9 compares experimental data in Ref. [18] with values calculated with the SW EoS for MM for the liquid phase isobaric heat capacity C_P^L. Values calculated with the PRSV EoS are also included to compare the performance of the two models. As expected the values computed with the SW equation of state are more accurate: the AAD between values calculated with the SW EoS and experimental C_P^L data is 0.50%, whereas for the PRSV EoS it is 3.0%.

Table 16
Deviation between the experimental values for v_c [14] and the value calculated with the newly developed 12-parameter Span–Wagner EoS for MM

v_c from EoS (m^3/kg)	v_c from Ref. [14] (m^3/kg)	$\varepsilon(v_c)$ from Ref. (%) [14]	DEV $= 100 \left\lvert \frac{v_{c\,\mathrm{DIPPR}} - v_{c\,\mathrm{EoS}}}{v_{c\,\mathrm{DIPPR}}} \right\rvert$ (%)
0.003285	0.003529–0.003874	25	6.9–15

ε is the uncertainty of the reference data.

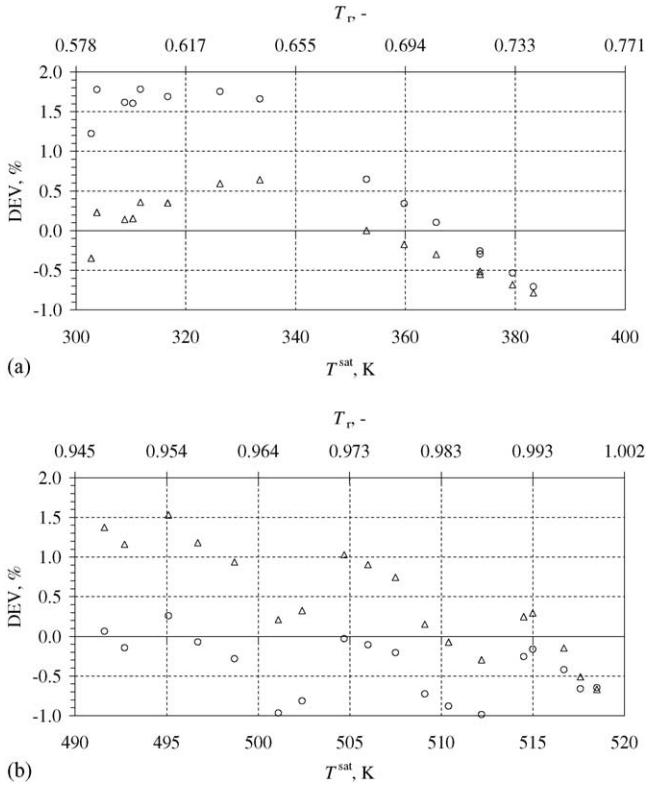

Fig. 8. Deviations between experimental and calculated vapor pressure data for MM. The percentage deviation is defined as: DEV = $100((P^{sat}_{exp} - P^{sat}_{calc})/P^{sat}_{exp})$. (◯) PRSV EoS and (△) new SW EoS. Comparison with experimental data from: (a) Ref. [27] and (b) Ref. [15].

- *Gas phase P–v–T data*. The detailed comparison between the values calculated by the SW and PRSV EoS's is reported in Appendix A (Table A.2). Also included in the tables is the value for the compressibility factor Z, which gives an indication of the non-ideality of the measured points ($Z_{min} = 0.88$). Both EoS's perform satisfactorily: the AAD for the SW EoS is 0.73%, while for the PRSV is 0.33%.
- *Liquid phase P–v–T data*. Table A.1 in Appendix A reports the deviations between calculated and experimental orthobaric specific volume data at 1 atm in the liquid phase reported in Ref. [32]. The SW EoS for MM performs better than the PRSV EoS in representing the experimental data: the values calculated with the PRSV EoS deviate from experimental data by as much as 5.17%, while the maximum deviation for values calculated with the SW EoS for MM is 0.27%.

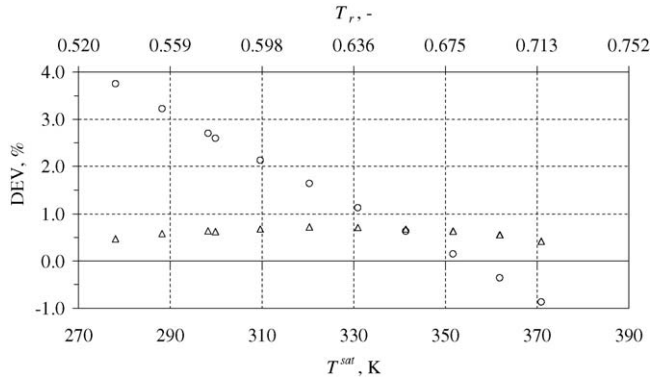

Fig. 9. Deviations between experimental [18] and calculated saturated liquid C_P data for MM. The deviation is defined as: DEV = $100((C^{L}_{P,exp} - C^{L}_{P,calc})/C^{L}_{P,exp})$. (◯) PRSV EoS and (△) new SW EoS.

Table 17 summarizes the performance of the SW EoS for MM.

5.2.2. Tetradecamethylhexasiloxane, MD_4M ($C_{14}H_{42}O_5Si_6$)

The available experimental data for MD_4M include critical point data, orthobaric liquid specific volumes, and experimental vapor pressures.

- *Critical point*. Table 18 lists the deviation between the computed value for v_c and estimated/experimental data [14]. Also included is the uncertainty in the estimated/experimental values. There is a large uncertainty in the literature values of the critical specific volume, and the value calculated by the EoS has a comparatively large deviation from the experimen-

Table 17
Summary of comparisons between experimental data sets used for the development of the new EoS for MM and calculated values

Source	No. of data points	P and T range		AAD (%)	
		T (K)	P (MPa)	Gas phase/liquid phase	Saturated state
Vapor pressure					
[15]	15	302–385	–	–	0.39
[19]	11	490–519	–	–	0.65
Saturated liquid heat capacity					
[18]	20	208–371	–	–	0.50
Low pressure gas heat capacity					
[18]	11	360–500	0–0.001	0.45	–
Low pressure P–v–T data					
[24]	43	448–573	0.06–0.3	0.69	–
[32]	11	300–357	0.101325	0.27	–

Table 18
Deviation between the estimated value for v_c [14] and the value calculated with the 12-parameter Span–Wagner EoS for MD_4M

v_c from EoS (m^3/kg)	v_c from Ref. [14] (m^3/kg)	$\varepsilon(v_c)$ from Ref. [14] (%)	DEV = $100\left\lvert\frac{v_{c\,DIPPR}-v_{c\,EoS}}{v_{c\,DIPPR}}\right\rvert$ (%)
0.003501	0.003594–0.003939	10	2.6–13

ε is the uncertainty of the reference data.

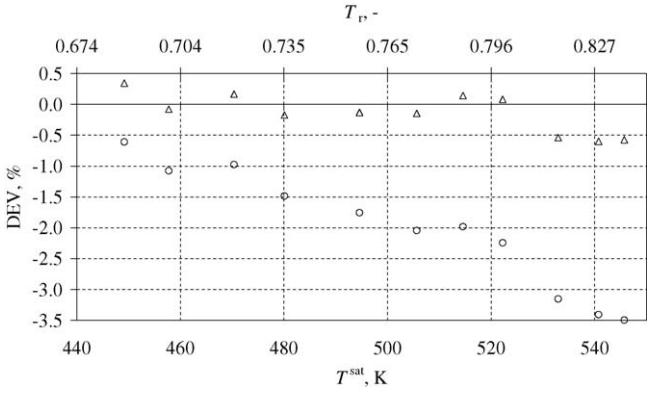

Fig. 10. Deviation between experimental [15] and calculated vapor pressures for MD_4M. The deviation is defined as: DEV = $100((P^{sat}_{exp} - P^{sat}_{calc})/P^{sat}_{exp})$. (◯) PRSV EoS and (△) new SW EoS.

Table 19
Summary of comparisons between experimental data sets used for the development of the new EoS for MD_4M and calculated values

Source	No. of data points	P and T range		AAD (%)
		T (K)	P (MPa)	
Vapor pressure				
[15]	11	449–546	–	0.27
Liquid phase P–v–T data				
[32]	11	300–412	0.101325	0.27

tal values. However, the obtained v_c is very close to other experimental values found in the literature (see Table 3).

- *Vapor pressure*. Experimental vapor pressure data for MD_4M are available only at low reduced pressures [15], namely up to 1.3 bar, i.e., $P_r \approx 0.15$. Fig. 10 graphically depicts the deviations between measurements and values calculated from both the new SW EoS and the PRSV cubic EoS. The results indicate that the PRSV EoS has an AAD of 2.0%, while for the SW EoS, the AAD is found to be 0.27%.
- *Liquid phase P–v–T data*. Table A.3 in Appendix A lists the deviations between the experimental and calculated values for the liquid phase specific volumes measured at a pressure of 1 atm. Results indicate that the PRSV EoS has a poorer performance (DEV_{max} = 4.94%) with respect to the newly developed SW EoS for MD_4M (DEV_{max} = 0.49%), even at a moderately low pressure.

Table 19 gives the AAD between experimental and predicted data from the new SW EoS.

5.2.3. Octamethylcyclotetrasiloxane, D_4 ($C_8H_{24}O_4Si_4$)

Among the siloxanes considered in this project, D_4 is possibly the most extensively measured fluid. Available experimental data for D_4 include critical point data, vapor pressures, saturated liquid specific volumes, and saturated and subcooled liquid sound speed data. Experimental saturated vapor specific volumes are also available [20], but are found to contain large systematic errors and therefore are excluded from the EoS parameters' optimization and from the EoS evaluation.

- *Critical point*. Table 20 lists the value for the computed critical specific volume and the range of experimental values. Based on the estimated uncertainty of the literature data [14], the reported value for v_c, as obtained from the SW EoS for D_4, is deemed acceptable for current technical applications.
- *Vapor pressure*. The measured saturated vapor pressures, reported in Refs. [15,20,48], are compared with values calculated with both the SW EoS and the PRSV cubic EoS in Fig. 11. The performance of the newly developed SW EoS for D_4 is on average better over the whole temperature range.
- *Saturated liquid specific volume*. Fig. 12 reports the deviations between experimental and calculated saturated liquid specific volume data (see Refs. [20,33]). As expected, the PRSV EoS has poorer performance in computing saturated liquid specific volumes; the deviations increase as the temperature approaches the critical temperature. The deviation between the values calculated by the SW EoS and measurements is <1.5% for all the points.
- *Liquid phase sound speed*. Experimental sound speed data are reported by Niepmann and Schmidt [34]. The superior performance of the newly developed SW EoS compared to the PRSV

Table 20
Deviation between the estimated value for v_c in Ref. [14] and the value calculated using the new SW EoS for D_4

v_c from EoS (m^3/kg)	v_c from Ref. [14] (m^3/kg)	$\varepsilon(v_c)$ from Ref. [14] (%)	DEV = $100\left\lvert\frac{v_{c\,DIPPR}-v_{c\,EoS}}{v_{c\,DIPPR}}\right\rvert$ (%)
0.003257	0.003270–0.003317	5	0.41–1.9

ε is the uncertainty of the reference data.

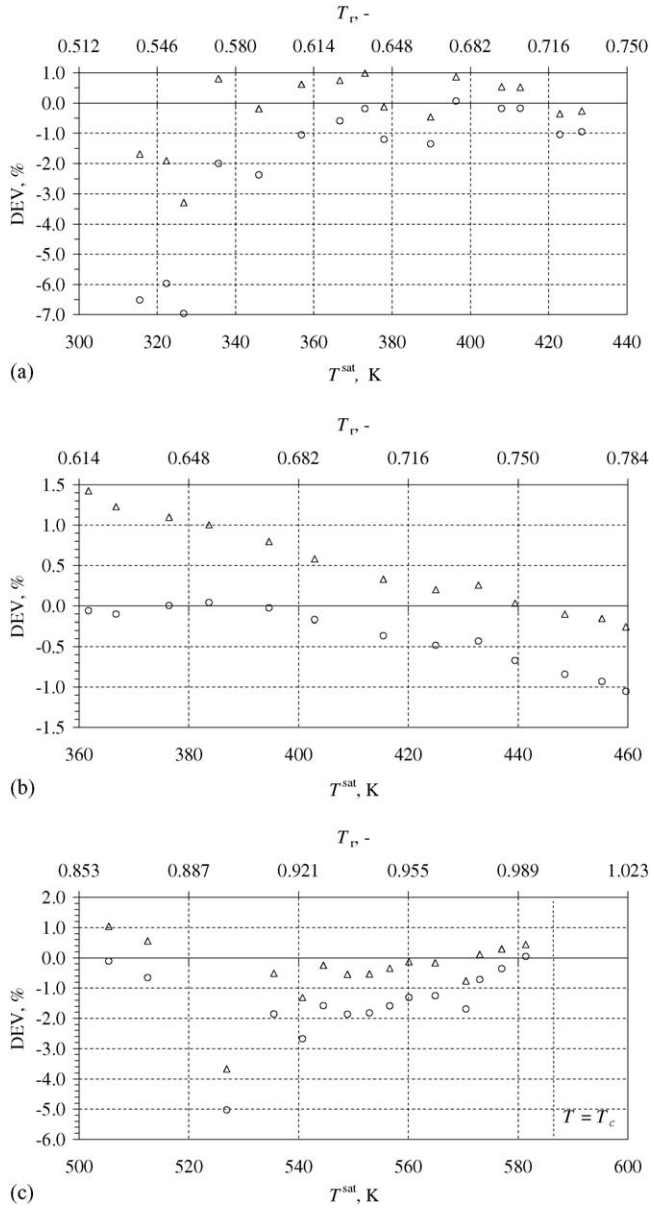

Fig. 11. Deviation between experimental and calculated vapor pressure data for D_4. The percentage deviation is defined as: $DEV = 100((P^{sat}_{exp} - P^{sat}_{calc})/P^{sat}_{exp})$. (◯) PRSV EoS and (△) new SW EoS. Comparison with experimental data from: (a) Ref. [48], (b) Ref. [15], and (c) Ref. [20].

EoS in computing sound speeds in the saturated and subcooled liquid phase is illustrated in Fig. 13. Note that the sound speed is a caloric property and thus depends on the isobaric ideal gas specific heat capacity C^{ig}_P. As previously indicated in Section 3.3, the adopted correlation for $C^{ig}_P(T)$ is affected by an estimated uncertainty of 25%. However, a simple sensitivity study (see Section 6) indicates that the liquid phase sound speed is not significantly influenced by the mentioned uncertainty.

- *Subcooled liquid density*. In the subcooled liquid phase, the new SW EoS predicts all available experimental liquid density data within 0.95%, whereas the PRSV EoS predicts all available liquid densities within 1.5%.

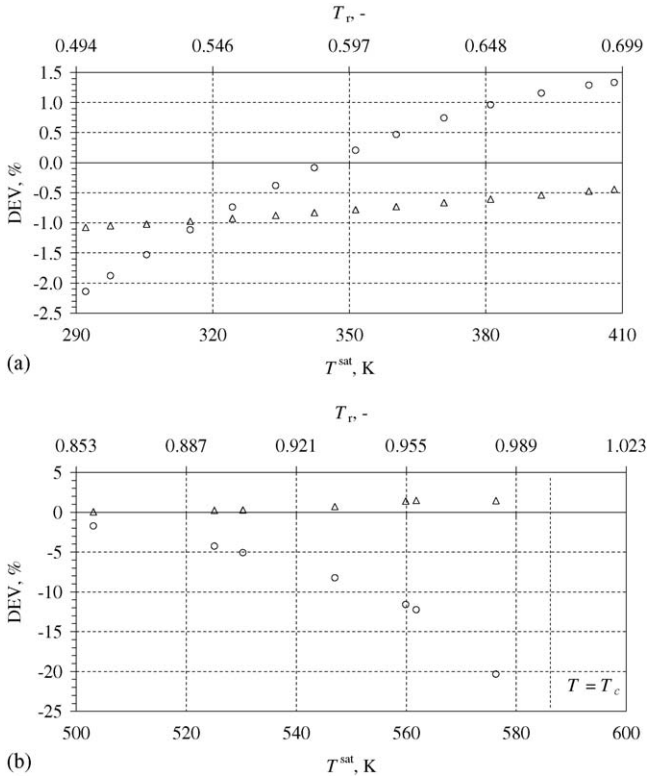

Fig. 12. Deviation between predicted and experimental saturated liquid density/specific volume data for D_4. The percentage deviation is defined as: $DEV = 100((v^L_{exp} - v^L_{calc})/v^L_{exp})$. (◯) PRSV EoS and (△) new SW EoS. Comparison with experimental data from: (a) Ref. [33] and (b) Ref. [20].

A summary of the performance of the SW EoS for D_4 is given in Table 21.

5.2.4. *Decamethylcyclopentasiloxane, D_5 ($C_{10}H_{30}O_5Si_5$)*

Only experimental vapor pressures and saturated liquid specific volumes are reported for D_5 (see Refs. [15,33]).

- *Critical point data*. The critical specific volume determined from the new SW EoS for D_5 is listed in Table 22. The result shows that the calculated critical specific volume is within the uncertainty assigned by DIPPR and is thus deemed acceptable within the scope of this project.
- *Vapor pressure*. Experimental vapor pressure data for D_5 are compared with data calculated using both the new SW EoS and the PRSV cubic EoS. The results are shown in Fig. 14. On average, the PRSV EoS estimates the experimental values with an average absolute deviation of 1.3%, whereas the new SW EoS for D_5 estimates the same data with an average absolute deviation of 0.27%.
- *Saturated liquid density*. Fig. 15 shows the deviations between the calculations of v^L made with the new EoS and experimental data in Ref. [33]. Computations made with the PRSV EoS are indicated to assess the improvement. The new SW EoS for D_5 calculates the liquid densities at the same temperature as the experimental data with an average absolute deviation of 0.60%, while the PRSV estimates have an average absolute deviation of 5.0%.

Table 21
Summary of comparisons between experimental data sets used for the development of the new EoS for D_4 and calculated values

Source	No. of data points	P and T range		AAD (%)	
		T (K)	P (MPa)	Subcooled liquid	Saturated state
Liquid P–v–T data					
[35]	36	308–427	10–180	0.20	–
[36]	6	313–413	0.1	0.63	–
Vapor pressure					
[15]	13	360–460	–	–	0.57
[48]	16	303–428	–	–	0.89
[20]	16	505–586	–	–	0.71
Saturated liquid density					
[33]	14	292–408	–	–	0.78
[20]	7	503–576	–	–	0.80
Saturated liquid sound speed					
[34]	18	303–440	–	–	1.5
Subcooled liquid sound speed					
[34]	135	300–450	1×10^{-4} to 24	1.1	–

Table 22
Deviation between the estimated value for v_c [14] and the predicted value from the new 12-parameter Span–Wagner functional form for D_5

v_c from EoS (m^3/kg)	v_c from Ref. [14] (m^3/kg)	$\varepsilon(v_c)$ from Ref. [14] (%)	$\mathrm{DEV} = 100 \left\lvert \frac{v_{c\,\mathrm{DIPPR}} - v_{c\,\mathrm{EoS}}}{v_{c\,\mathrm{DIPPR}}} \right\rvert$
0.003418	0.003210–0.003479	10	−6.5–1.7

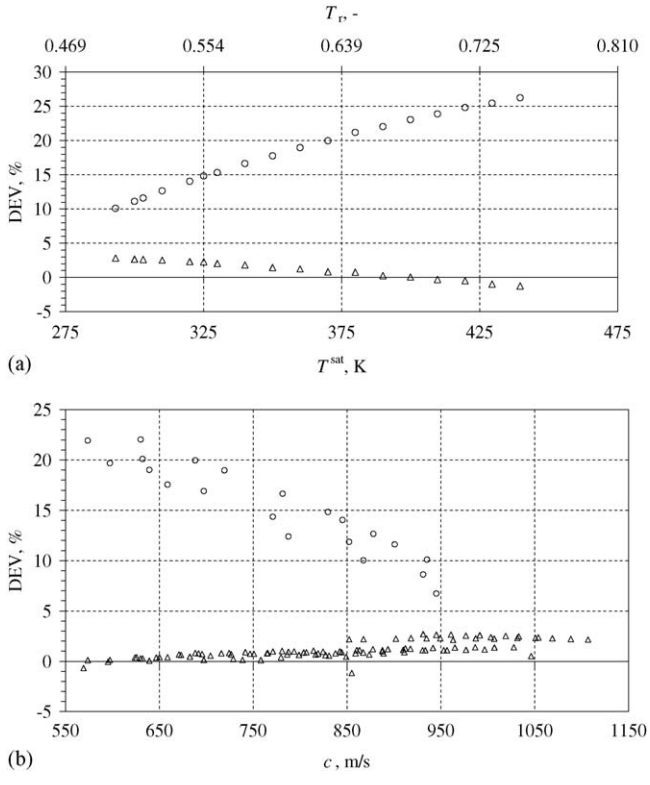

Fig. 13. Deviation between experimental and calculated liquid sound speed data for D_4. (◯) PRSV EoS and (△) new SW EoS. (a) Comparison with saturated liquid sound speed data in Ref. [34]. The percentage deviation is defined as: $\mathrm{DEV} = 100((c^{L}_{exp} - c^{L}_{calc})/c^{L}_{exp})$. (b) Comparison with subcooled liquid sound speed data in Ref. [34]. The percentage deviation is defined as: $\mathrm{DEV} = 100((c_{exp} - c_{calc})/c_{exp})$.

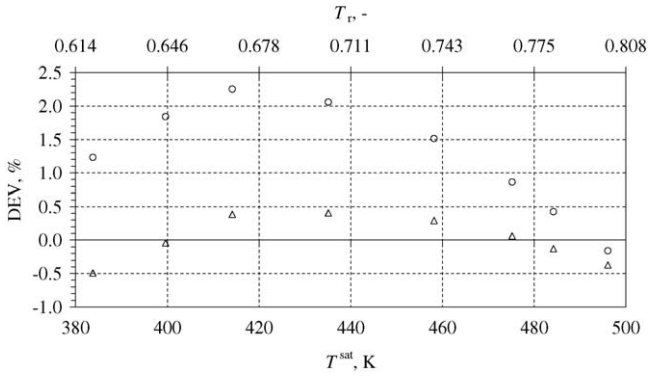

Fig. 14. Deviation between experimental [15] and calculated vapor pressures for D_5. The percentage deviation is defined as: $\mathrm{DEV} = 100((P^{sat}_{exp} - P^{sat}_{calc})/P^{sat}_{exp})$. (◯) PRSV EoS and (△) new SW EoS.

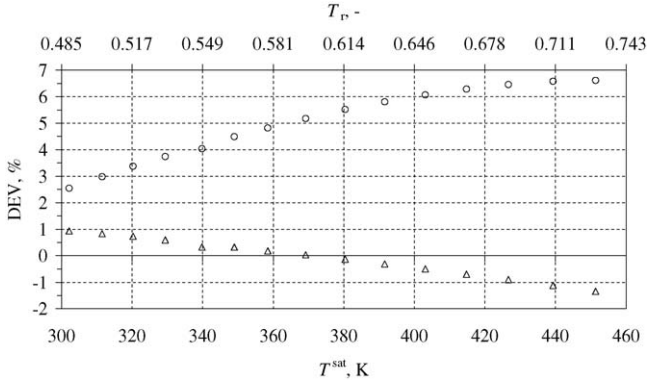

Fig. 15. Deviation between experimental [33] and calculated saturated liquid densities/specific volumes for D_5. The percentage deviation is defined as: $\mathrm{DEV} = 100((v^{L}_{exp} - v^{L}_{calc})/v^{L}_{exp})$. (◯) PRSV EoS and (△) new SW EoS.

Table 23
Summary of comparisons between experimental data sets used for the development of the new EoS for D_5 and calculated values

Source	No. of data points	P and T range		AAD (%)
		T (K)	P (MPa)	
Vapor pressure				
[15]	8	380–497	–	0.27
Saturated liquid density				
[33]	15	300–452	–	0.60

The performance of the new SW EoS for D_5 is illustrated in Table 23.

6. Sensitivity of caloric properties to the uncertainty in the isobaric ideal gas heat capacity

The isobaric ideal gas heat capacity correlation, necessary for the computation of caloric properties, e.g., sound speed, enthalpy, and entropy, is affected by an estimated uncertainty of about 25%, assumedly over the entire temperature range of validity of the newly developed EoS's for siloxanes, namely 300–673 K. In this section, the assessment of the sensitivity of the estimation of caloric properties using the new SW EoS's to the mentioned uncertainty is described. Note that volumetric properties are unaffected by the uncertainty in the C_P^{ig} correlation [46].

6.1. Sensitivity of the sound speed to the uncertainty in C_P^{ig}

The sensitivity of the sound speed is analyzed in the following thermodynamic regions/states:

- ideal gas region;
- saturated vapor and liquid states;
- subcooled liquid region;
- dense gas region.

In the ideal gas state the sound speed is given by $c = \sqrt{\gamma RT}$, where $\gamma \equiv C_P^{ig}/C_v^{ig}$ is the ratio of the isobaric ideal gas specific heat to the isochoric ideal gas specific heat. In the case of complex molecules like siloxanes, γ is close to unity and thus $c \simeq \sqrt{RT}$, e.g., at 500 K γ of D_4 is 1.06, computed using the current heat capacity correlation (see Table 10). With a −25% uncertainty, γ of D_4 becomes 1.08. This implies that for complex molecules, the ideal gas sound speed is practically insensitive to the uncertainty in the C_P^{ig} correlation.

The following procedure is adopted to estimate the uncertainty in the saturated vapor and liquid sound speed:

- first, the sound speed is computed from the current isobaric ideal gas heat capacity correlation;
- next, using the 25% uncertainty in the C_P^{ig} correlation, the saturated vapor and liquid sound speed are computed;
- these values are then compared with the results from the first step.

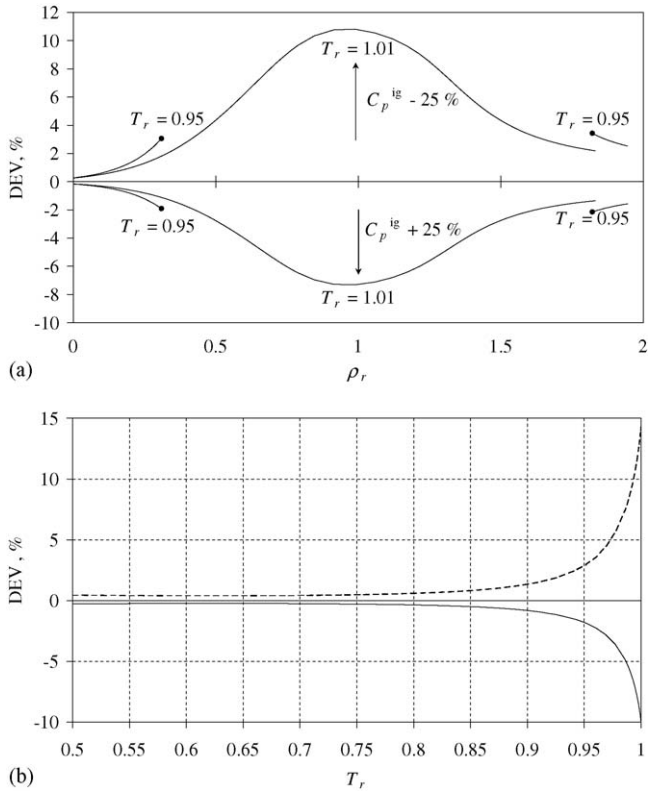

Fig. 16. Sensitivity of the calculated sound speed c to the uncertainty in the adopted correlation for the isobaric ideal gas heat capacity, i.e., $C_P^{ig} \pm 25\%$. DEV = $100((c - c_{ref})/c_{ref})$. (a) Near critical isotherms. (b) Saturated vapor. (- - -) Values calculated for $C_P^{ig} + 25\%$ and (—) values calculated for $C_P^{ig} - 25\%$.

The results thus obtained show that the saturated sound speed differs by less than 3% for a change in C_P^{ig} of ±25% up to a reduced pressure of 0.9 (see Fig. 16). Fig. 16 also shows the sensitivity of the sound speed in the saturated vapor and liquid states to the uncertainty in the isobaric ideal gas heat capacity. The results indicate that the critical region is the most sensitive to the uncertainty in C_P^{ig}.

6.2. Sensitivity of the enthalpy and entropy changes between state points to the uncertainty in C_P^{ig}

Values for enthalpy and entropy can be obtained from the Helmholtz function by means of differentiation of the functional form with respect to its canonical variables, namely T and ρ (see details in Ref. [46]). Since only enthalpy and entropy differences are of importance for the design and analysis of many technical applications, only the sensitivity of Δh and Δs to the uncertainty in C_P^{ig} is investigated in the same thermodynamic regions as for the sound speed. The sensitivity is evaluated for isobaric, isothermal, and isochoric processes.

For isobaric processes, the following relations are valid:

$$\left(\frac{\partial s}{\partial T}\right)_P = \frac{C_p}{T} \quad \text{and} \quad \left(\frac{\partial h}{\partial T}\right)_P = C_p. \tag{8}$$

The change in entropy is obtained from:

$$\Delta s_P = \int_{T_1}^{T_2} \frac{C_P}{T}\,\mathrm{d}T. \tag{9}$$

The isobaric specific heat is related to the isochoric specific heat as

$$C_P = C_v + T\left(\frac{\partial v}{\partial T}\right)_P \left(\frac{\partial P}{\partial T}\right)_v. \tag{10}$$

Since the last term in this equation is independent of the heat capacity, $\varepsilon(C_P) = \varepsilon(C_v) = \varepsilon(C_v^{\mathrm{ig}}) = \varepsilon(C_P^{\mathrm{ig}})$, or

$$\frac{\varepsilon(C_P)}{C_P} = \frac{\varepsilon(C_P^{\mathrm{ig}})}{C_P}. \tag{11}$$

The value of C_P is always greater than C_v and C_v^{ig}. The lowest value of C_P occurs at the lower temperature boundary of the range of validity for the newly developed EoS's, i.e., 300 K. This means that the largest relative uncertainty in C_P is $(\varepsilon(C_P)/C_P)|_{\max} = (\varepsilon(C_v^{\mathrm{ig}}))/(C_P(> C_P^{\mathrm{ig}})) \approx (\varepsilon(C_v^{\mathrm{ig}}))/C_P^{\mathrm{ig}} = (\varepsilon(C_P^{\mathrm{ig}}))/C_P^{\mathrm{ig}} \to 25\%$. Substituting this result into Eq. (9), it can be shown that

$$\Delta s_P = 1 \pm k \int_{T_1}^{T_2} \frac{C_P^{\mathrm{current}}}{T}\,\mathrm{d}T, \tag{12}$$

where $k = \pm 0.25$ is a measure of the uncertainty in the isobaric ideal gas heat capacity and superscript current 'current' refers to the adopted heat capacity correlation. Note that it has been assumed that the uncertainty in C_P^{ig} is approximately 25% for all temperatures, i.e., k is independent of T. Eq. (12) thus indicates that the largest possible uncertainty in the entropy difference is 25% for the lower bound of the temperature range of validity of the EoS's. The same conclusions are valid for the enthalpy difference between two states for an isobaric process.

For isothermal processes the following equations are valid:

$$\begin{aligned} \left(\frac{\partial s}{\partial v}\right)_T &= \left(\frac{\partial P}{\partial T}\right)_v, \\ \left(\frac{\partial h}{\partial P}\right)_T &= v - T\left(\frac{\partial v}{\partial T}\right)_P. \end{aligned} \tag{13}$$

The right-hand sides of equation set (13) contain only volumetric properties, i.e., they are independent of the heat capacity. This means that for isothermal processes, the entropy and enthalpy changes are unaffected by the uncertainty in the C_P^{ig} correlation. This conclusion is also valid in the vapor–liquid equilibrium region.

For isochoric processes the following equations are valid:

$$\begin{aligned} \left(\frac{\partial s}{\partial T}\right)_v &= \frac{C_v}{T} \\ \left(\frac{\partial h}{\partial T}\right)_v &= C_P + \left[v - T\left(\frac{\partial v}{\partial T}\right)_P\right]\left(\frac{\partial P}{\partial T}\right)_v \end{aligned} \tag{14}$$

Using the procedure outlined for isobaric processes, it can be demonstrated that the relative uncertainty in Δh and Δs is about 25%.

An improvement in the estimation of the isobaric ideal gas heat capacity for siloxanes is one of the first steps to be taken to increase the accuracy of the estimation of properties relevant to technical applications.

7. Summary

Work related to the development of accurate equations of state for four siloxanes, namely MM, MD_4M, D_4, and D_5, has been presented. The selected functional form is the one by Span and Wagner expressed in terms of the Helmholtz free energy. The first part of the article describes the critical evaluation of experimental data and the calculation of additional thermodynamic points by means of ad hoc estimation methods. These predicted values are included in the optimization of the EoS parameters. A short review of the optimization procedure is also given. Finally, results from the optimization are presented. The procedure uses as input data the selected experimental values and the estimated points, appropriately weighted. A greater number of experimental data are available for MM and D_4, which are also more accurate on average if compared to the data for MD_4M and D_5. For this reason the resulting thermodynamic models for MM and D_4 are deemed more accurate than the ones for MD_4M and D_5. The second part of this paper deals with the performance of the developed Span–Wagner equations of state. The analysis of the performance is based on calculations of the average absolute deviations between experimental and calculated data and by means of visual information provided in state diagrams. The analysis also compares the performance of the new EoS's with the PRSV cubic equation of state. This equation of state was previously used in thermodynamic studies of energy applications employing siloxanes as working fluids. A simple analysis of the sensitivity of caloric properties to the current large uncertainty (25%) in the available estimates of the isobaric ideal gas heat capacity is also reported. Simple computations indicate that, depending on the thermodynamic region, the uncertainties in estimated caloric properties can be as high as 25%. Accurate measurements of the speed of sound in the vapor phase are planned for the near future. Together with the use of ab initio molecular simulations for the estimation of the isobaric ideal heat capacity, this should greatly reduce the uncertainty and improve the performance of the new EoS's for siloxanes.

Acknowledgements

The authors gratefully recognize the help of their friend and colleague Teus van der Stelt for his fundamental contribution to

the improvement of FluidProp. The authors are also grateful to D. Morgan of the Dow Corning Corporation for many fruitful exchanges.

List of symbols

A	substance-dependent parameter in the Daubert equation, Eq. (3) (kg/m^3)
B	substance-dependent parameter in the equation by Daubert
c	substance-dependent parameter in the Wagner–Ambrose equation
C	substance-dependent parameter in the equation by Daubert (K)
C_P	isobaric specific heat (kJ/(kmol K))
C_v	isochoric specific heat (kJ/(kmol K))
D	substance-dependent parameter in the equation by Daubert
h	enthalpy (kJ/kg)
MW	molecular weight (kg/kmol)
$n_1, \ldots, n_{12}$	adjustable parameters in the Span–Wagner functional form, Eq. (7)
P	pressure (bar)
R	universal gas constant, 8.314472 kJ/(kmol K)
s	entropy (kJ/(kmol K))
T	absolute temperature (K)
v	specific volume (m^3/kg)
x	vapor quality
Z	compressibility factor

Greek letters

δ	reduced density
$\varepsilon(Q)$	uncertainty in property Q, unit is property dependent
γ	ratio of the isobaric to the isochoric heat capacity
η_1	substance-dependent parameter in the C_P^{ig} correlation, Eq. (4) (kJ/(kmol K))
η_2	substance-dependent parameter in the C_P^{ig} correlation (kJ/(kmol K^2))
η_3	substance-dependent parameter in the C_P^{ig} correlation (kJ/(kmol K^3))
η_4	substance-dependent parameter in the C_P^{ig} correlation (kJ/(kmol K^4))
ρ	fluid density (kg/m^3)
τ	inverse of the reduced temperature
ω	acentric factor
ω_1	substance-dependent parameter in the Wagner–Ambrose equation, Eq. (1)
ω_2	substance-dependent parameter in the Wagner–Ambrose equation
ω_3	sound speed (m/s)
ω_4	substance-dependent parameter in the Wagner–Ambrose equation
ψ	reduced Helmholtz energy
Ψ	Helmholtz energy (kJ/kg)

Subscripts

B	boiling point
c	critical
calc	calculated value
exp	experimental value
r	reduced
ref	reference
TP	triple point
MP	melting point
vap	vaporization

Superscripts

ig	ideal gas
L	saturated liquid
r	residual
sat	saturated
V	saturated vapor

Appendix A

Table A.1
Comparison between orthobaric liquid phase P–v–T data for MM in Ref. [32] and values calculated with the newly developed SW EoS and the PRSV cubic EoS

T_{exp} (K)	v_{exp} (cm^3/g)	DEV $= 100 \left\lvert \frac{v_{exp}-v_{calc}}{v_{exp}} \right\rvert$ (%)	
		Span–Wagner	PRSV EoS
278.501	1.27745	0.70	4.19
299.468	1.3145	0.41	4.80
302.544	1.32017	0.37	4.88
305.07	1.32487	0.34	4.94
310.386	1.33495	0.26	5.06
315.355	1.34456	0.20	5.16
320.358	1.35444	0.13	5.25
330.477	1.37514	0.01	5.40
334.984	1.38463	0.07	5.45
339.489	1.39437	0.13	5.49
345.983	1.40879	0.21	5.54
351.993	1.42256	0.29	5.55
357.957	1.43672	0.37	5.55

Table A.2
Comparison between gas phase P–v–T data for MM in Ref. [24] and values calculated with the newly developed SW EoS and the PRSV cubic EoS (only selected data)

T_{exp} (K)	P_{exp} (bar)	v_{exp} (m^3/kg)	DEV $= 100 \left\lvert \frac{v_{exp}-v_{calc}}{v_{exp}} \right\rvert$ (%)		Z[a]
			Span–Wagner	PRSV	
448.26	0.6462	0.3462	0.63	0.48	0.97
	0.8107	0.2749	0.51	0.32	0.97
	0.9633	0.2301	0.56	0.34	0.97
	1.1151	0.1981	0.46	0.21	0.96
	1.3116	0.1670	0.67	0.39	0.95
	1.5831	0.1370	0.75	0.43	0.94
	1.8674	0.1147	0.97	0.61	0.93
	2.0308	0.1046	1.29	0.90	0.93
	3.1136	0.0661	0.25	0.22	0.90
	3.3386	0.0611	0.29	0.18	0.89
	3.5955	0.0560	0.41	0.05	0.88
498.28	0.7246	0.3471	0.06	0.21	0.99
	0.8673	0.2894	0.01	0.34	0.98
	0.9602	0.2606	0.10	0.26	0.98
	1.1067	0.2254	0.13	0.29	0.98
	1.4737	0.1676	0.41	0.15	0.97
	1.6755	0.1467	0.47	0.16	0.96
	1.8681	0.1311	0.46	0.24	0.96
	2.1903	0.1107	0.72	0.09	0.95
	3.6187	0.0651	0.45	0.87	0.92
523.15	0.7132	0.3682	0.91	0.62	0.98
	0.7886	0.3341	0.45	0.13	0.98
	0.9362	0.2808	0.43	0.05	0.98
	1.0474	0.2500	0.64	0.23	0.98
	1.2406	0.2104	0.68	0.19	0.97
	1.3959	0.1865	0.69	0.14	0.97
	1.6518	0.1567	0.86	0.21	0.97
	1.8915	0.1362	0.95	0.20	0.96
	2.1785	0.1173	1.24	0.38	0.95
	2.4433	0.1038	1.60	0.63	0.95
	3.7556	0.0669	0.11	1.34	0.94
548.04	0.7478	0.3691	0.73	0.43	0.98
	0.8915	0.3098	0.48	0.13	0.98
	1.0093	0.2731	0.51	0.12	0.98
	1.1341	0.2425	0.58	0.14	0.98
	1.4130	0.1939	0.62	0.07	0.98
	1.6400	0.1663	0.78	0.14	0.97
	1.8773	0.1445	0.96	0.23	0.97
	2.1718	0.1241	1.25	0.41	0.96
	2.3596	0.1141	1.14	0.22	0.96
	2.6543	0.1005	1.62	0.59	0.95
573.04	0.7615	0.3781	1.12	0.84	0.98
	0.9676	0.2983	0.67	0.30	0.98
	1.1256	0.2556	0.79	0.37	0.98
	1.4106	0.2035	0.74	0.22	0.98
	1.6745	0.1708	0.83	0.21	0.97
	1.9206	0.1481	1.10	0.39	0.97
	2.1983	0.1289	1.19	0.38	0.97
	2.4598	0.1146	1.41	0.51	0.96
	2.7606	0.1018	1.40	0.38	0.96
	2.9502	0.0953	1.10	0.02	0.96

[a] Z is calculated from the experimental data.

Table A.3
Comparison between atmospheric liquid phase P–v–T data reported by McLure et al. [32] for MD_4M and values calculated with the new SW EoS and the PRSV cubic EoS

T_{exp} (K)	v_{exp} (cm^3/g)	DEV $= 100 \left\lvert \frac{v_{exp}-v_{calc}}{v_{exp}} \right\rvert$ (%)	
		Span–Wagner	PRSV
303.092	1.13569	0.14	0.14
308.089	1.14192	0.45	0.15
312.967	1.14805	0.41	0.42
318.069	1.15452	0.37	0.70
323.103	1.16099	0.32	0.98
327.810	1.16704	0.28	1.22
333.881	1.17501	0.23	1.54
338.026	1.18051	0.19	1.76
343.137	1.18737	0.15	2.01
347.760	1.19363	0.11	2.24
352.900	1.20069	0.06	2.49
363.051	1.21493	0.03	2.96
372.923	1.22912	0.12	3.40
382.167	1.24286	0.21	3.80
392.352	1.25839	0.30	4.21
402.590	1.27457	0.40	4.60
411.903	1.2898	0.49	4.94

References

[1] G. Angelino, C. Invernizzi, Cyclic methylsiloxanes as working fluids for space power cycles, J. Sol. Energy—T. ASME 115 (3) (1993) 130–137.
[2] G. Angelino, P. Colonna, Multicomponent working fluids for Organic Rankine Cycles (ORCs), Energy 23 (6) (1998) 449–463.
[3] G. Angelino, P. Colonna, Organic Rankine Cycles for energy recovery from molten carbonate fuel cells, in: 35th Intersociety Energy Conversion Engineering (IECEC) Conference and Exhibit, Las Vegas, NV, AIAA, Reston, VA, 2000.
[4] G. Angelino, P. Colonna, Air cooled siloxane bottoming cycle for molten carbonate fuel cells, in: 2000 Fuel Cell Seminar, No. 114, Portland, OR, 2000, pp. 667–670.
[5] P. Colonna, P. Silva, Dense gas thermodynamic properties of single and multi-component fluids for fluid dynamics simulations, J. Fluids Eng. 125 (3) (2003) 414–427.
[6] P. Colonna, S. Rebay, Numerical simulation of dense gas flows on unstructured grids with an implicit high resolution upwind Euler solver, Int. J. Numer. Meth. Fluids 46 (7) (2004) 735–765.
[7] B.P. Brown, B.M. Argrow, Application of Bethe–Zel'dovic–Thompson fluids in Organic Rankine Cycle engines, J. Propul. Power. 16 (6) (2000) 1118–1123.
[8] R. Span, W. Wagner, Equations of state for technical applications. I. Simultaneously optimized functional forms for nonpolar and polar fluids, Int. J. Thermophys. 24 (1) (2003) 1–39.
[9] E.W. Lemmon, R. Span, Short fundamental equations of state for 20 industrial fluids, J. Chem. Eng. Data 51 (3) (2006) 785–850.
[10] H. van Putten, P. Colonna, Dynamic model of a small biomass fired steam power plant, in: 3rd International Energy Conversion Engineering Conference (IECEC), No. 2005-5638, AIAA, 2005.
[11] R. Gnutek, P. Colonna, Modular lumped-parameters dynamic model for gas turbines: validation and application to a small scale externally fired gas turbine, in: 2005 ASME International Mechanical Engineering Congress and Exposition (IMECE), No. 2005-80720, ASME, 2005.
[12] R. Stryjek, J.H. Vera, PRSV: an improved Peng–Robinson equation of state for pure compounds and mixtures, Can. J. Chem. Eng. 64 (1986) 323–333.
[13] P. Colonna, T. van der Stelt, FluidProp V. 1: A Program for the Estimation of Thermophysical Properties of Fluids, Software, 2005, www.fluidprop.com.

[14] R. Rowley, W. Wilding, J. Oscarson, Y. Yang, N. Zundel, T. Daubert, R. Danner, DIPPR Data Compilation of Pure Chemical Properties, Taylor & Francis Publishing Company, New York, NY, 2004.
[15] O.L. Flaningam, Vapor pressures of poly(dimethylsiloxane) oligomers, J. Chem. Eng. Data 31 (1986) 266–272.
[16] A. Guardone, P. Colonna, Available Thermodynamic Data on Linear and Cyclic Siloxanes (Version 1), Scientific Report ET-2178, Delft University of Technology, Process and Energy Department, Energy Technology Section, Mekelweg 2, 2628 CD Delft, The Netherlands, April 2005.
[17] M. Frenkel, Q. Dong, R.C. Wilhoit, K.R. Hall, TRC SOURCE database: a unique tool for automatic production of data compilations, Int. J. Thermophys. 22 (2001) 215–226.
[18] D.W. Scott, J.F. Messerly, S.S. Todd, G.B. Guthrie, I.A. Hossenlopp, R.T. Moore, A. Osborn, W.T. Berg, J.P. McCullough, Hexamethyldisiloxane: chemical thermodynamic properties and internal rotation about the siloxane linkage, J. Phys. Chem. 65 (1961) 1320–1326.
[19] I.A. McLure, E. Dickinson, Vapour pressure of hexamethyldisilixane near its critical point: corresponding-states principle for dimethylsiloxanes, J. Chem. Thermodyn. 8 (1976) 93–95.
[20] C. Young, Equilibrium properties of octamethylcyclotetrasiloxane near its critical point and applicability of the principle of corresponding states, J. Chem. Thermodyn. 4 (1972) 65–75.
[21] E. Dickinson, I.A. McLure, Thermodynamics of *n*-alkane + dimethylsiloxane mixtures. Part 1. Gas–liquid critical temperatures and pressures, J. Chem. Soc., Faraday Trans. 1 70 (1974) 2313–2320.
[22] C.L. Young, Critical properties of mixtures containing siloxanes, J. Chem. Soc., Faraday Trans. 2 68 (1972) 452–459.
[23] I.A. McLure, J.F. Neville, The critical temperature and pressures of hexamethyldisilmethylene, octamethylcyclotetrasiloxane and decamethylcyclopentasiloxane, J. Chem. Thermodyn. 14 (1982) 385–388.
[24] D. Marcos, D. Lindley, K. Wilson, W. Kay, H. Hershey, A (*P*, *v*, *T*) study of tetramethylsilane, hexamethyldisiloxane, octamethyltrisiloxane, and toluene from 423 K to 573 K in the vapor phase, J. Chem. Thermodyn. 15 (1983) 1003–1014.
[25] D.F. Wilcock, Vapor pressure–viscosity relations in methylpolysiloxanes, J. Am. Chem. Soc. 68 (1946) 691–696.
[26] K.K.S. Mekhtiev, Analysis of the results of thermodynamic studies of a series of organosilixon compounds, Azerb. Khim. Zhur. 5 (1981) 85–88.
[27] R.C. Osthoff, W.T. Grubb, C.A. Burkhard, Physical properties of organosilicon compounds. I. Hexamethylcyclotrisiloxane and octamethylcyclotetrasiloxane, J. Am. Chem. Soc. 75 (1954) 2227–2229.
[28] J. Lipowitz, M.J. Ziemelis, Flammability and fire hazard properties of poly(dimethylsiloxanes). Am. Chem. Soc. Div. Org. Coat. Plast. Chem. Prepr. 36 (2) (1976) 582–586.
[29] C. Hicks, C. Young, Critical properties of binary mixtures, J. Chem. Soc., Faraday Trans. 1 72 (1976) 122–133.
[30] R.S. Myers, H.L. Clever, Surface tension of octamethylcyclotetrasiloxane and hexamethyldisilazane and their solutions with carbon tetrachloride and *n*-hexadecane, J. Chem. Eng. Data 14 (2) (1969) 161–164.
[31] T. Alvik, J. Dale, On the lack of conformational preferences for cyclic dimethylsiloxane oligomers, Acta Chem. Scand. (1971) 2131.
[32] I.A. McLure, A.J. Pretty, P.A. Sadler, Specific volumes, thermal pressure coefficients, and derived quantities of five dimethylsiloxane oligomers from 25 to 140 °C, J. Chem. Eng. Data 22 (4) (1977) 372–376.
[33] I.A. McLure, J.-M. Barbarin-Castillo, Orthobaric liquid densities for octamethylcyclotetrasiloxane, decamethylcyclopentasiloxane, dimethicone 20, and a cyclic poly(dimethylsiloxane), J. Chem. Eng. Data 39 (1994) 12–13.
[34] R. Niepmann, U. Schmidt, Speeds of sound in liquid octamethylcyclotetrasiloxane, J. Chem. Thermodyn. 12 (12) (1980) 1133–1137.
[35] S. Wappmann, I. Tarassov, H. Liidemann, Densities of octamethylcyclotetrasiloxane + methane and 2,2-dimethylpropane + methane from 10 to 200 MPa and from 294 to 433 K, J. Chem. Eng. Data 41 (1996) 84–88.
[36] M.S. Benson, J. Winnick, Liquid phase PVTx properties of carbon tetrachloride-octamethylcyclotetrasiloxane binary mixtures, J. Chem. Eng. Data 21 (4) (1976) 432–443.
[37] D. Ambrose, The correlation and estimation of vapour pressures. IV. Observations on Wagner's method of fitting equations to vapour pressures, J. Chem. Thermodyn. 18 (1986) 45–51.
[38] B. Poling, J. Prausnitz, J. O'Connell, The Properties of Gases and Liquids, Chemical Engineering Series, fifth ed., McGraw-Hill, New York, 2001.
[39] J. Smith, H.V. Ness, M. Abbott, Introduction to Chemical Engineering Thermodynamics, McGraw-Hill International Edition, Singapore, 2001.
[40] E.W. Lemmon, M.L. Huber, Thermodynamic properties of *n*-dodecane, Energy Fuels 18 (2004) 960–967.
[41] M.M. Abbott, Cubic equations of state, AIChE J. 19 (1973) 596–601.
[42] D.H. Smith, M. Ferer, Improved phase boundary for one-component vapor–liquid equilibrium incorporating critical behavior and cubic equations of state, Fluid Phase Equilib. 113 (1995) 103–115.
[43] B. Harrison, W. Seaton, Solution to missing group problem for estimation of ideal gas heat capacities, Ind. Eng. Chem. Res. 27 (1988) 1536–1540.
[44] P. Colonna, Fluidi di lavoro multi componenti per cicli termodinamici di potenza (Multicomponent working fluids for power cycles), Ph.D. Thesis, Politecnico di Milano, October 1996.
[45] F.A. Aly, L.L. Lee, Self-consistent equations for calculating the ideal gas heat capacity, enthalpy, and entropy, Fluid Phase Equilib. 6 (1981) 169–179.
[46] R. Span, Multiparameter Equations of State—An Accurate Source of Thermodynamic Property Data, Springer-Verlag, Berlin, 2000.
[47] R. Span, W. Wagner, Equations of state for technical applications. II. Results for nonpolar fluids, Int. J. Thermophys. 24 (1) (2003) 41–109.
[48] R.C. Osthoff, W.T. Grubb, Physical properties of organosilicon compounds. III. Thermodynamic properties of octamethylcyclotetrasiloxane, J. Am. Chem. Soc. 76 (1953) 399–401.